Journal of Geophysical Research: Solid Earth

Supporting Information for

Bilateral heterogeneity in an upwelling mantle via double subduction of oceanic lithosphere

Nghiem Van Dao[1,2], Hiroshi Kitagawa[1*], Eizo Nakamura[1], Katsura Kobayashi[1], Thanh Xuan Ngo[2] and Son Hai Trinh[3]

[1]The Pheasant Memorial Laboratory for Geochemistry and Cosmochemistry, Institute for Planetary Materials, Okayama University, Misasa, Tottori, 682-0193, Japan

[2]Department of Geology, Hanoi University of Mining and Geology, Hanoi, Vietnam

[3]Vietnam Institute of Geoscience and Mineral resources, Hanoi, Vietnam

Text S1. Basement geology and crustal lithologies of Vietnam

The basement terrane of Indochina Peninsula consists of continental blocks, termed South China block and Indochina block. These blocks are allochthonous continental fragments derived from Gondwana, and composed of Proterozoic to Phanerozoic rocks of igneous, sedimentary, and metamorphic origins. Detailed geologic, petrologic, and geochemical studies have been conducted for some massifs or terranes; e.g., Tu Le basin and Phan Si Pan uplift in Northern Vietnam (Tran et al., 2015) and the Kontum massif in Central Vietnam (e.g., Lan et al., 2003).

The Kontum massif is the largest basement exposure in the Indochina block, and located in Central Vietnam. The massif consists of granitic rocks, felsic and mafic gneisses, charnockites, schist and amphibolite of Paleozoic to Mesozoic ages. The massif is, in part, overlain unconformably by Cenozoic basalts in the Song Cau region (Lepivrier et al., 2004; Maluski et al., 2005). Thus, these lithologies of the massif could be one of possible assimilants of the Cenozoic Vietnamese basalts. Geochemical and isotopic data of the massif rocks are provided in Lan et al. (2003), Owada et al. (2007) and Jiang et al. (2020).

The other, younger basement rocks, dominated by felsic igneous rocks, is exposed in the other areas in Vietnam. One of the igneous complexes, well studied and capped by Cenozoic basalts, is the Dalat zone in Southern Vietnam (Nguyen et al., 2004a, 2004b). The Dalat zone contains three suites of Cretaceous granitic batholiths, namely the Dinhquan suite, the Deoca suite and the Ankroet (or Cana) suite; the ages of these granitic rocks are 120–90 Ma (Nguyen et al., 2004a, 2004b; Shellnutt et al., 2013; Nguyen et al., 2021). The Dinhquan and Deoca granitic rocks are mostly metaluminous and classified into I-type granite, while the Ankroet granites are peraluminous and some are classified into A-type granite (Nguyen et al., 2004a; Shellnutt et al., 2013). Since these batholiths are partly capped by Cenozoic basalts distributed in Xuan Loc, Dalat and Phuoc Long, granitic rocks of the batholiths represent a possible assimilant in parental magmas of basalts in Southern Vietnam. Elemental and isotopic compositions of these basalts are given by Nguyen et al. (2004a) and Shellnutt et al. (2013).

Text S2. Analytical Methods

Samples were collected in the traverse from north to south of central and southern Vietnam for individual volcanic fields and 3 islands in the continental shelf of EVS/SCS (Figure S1). The geodetic coordinates and altitude of sampling locations were obtained using GPS (Global Positioning System). The least altered hand specimens were collected by using a sledgehammer then the weathered crusts of samples were removed by a picking hammer. Thin sections were made for all samples and carefully examined under an optical microscope. The fresh fractions were picked up for geochemical and geochronological analyses. All experiments were carried out at the Pheasant Memorial Laboratory (PML) for Geochemistry and Cosmochemistry, Institute for Planetary Materials (IPM), Okayama University at Misasa (Nakamura et al., 2003).

For whole rock analysis, samples were crushed by a jaw crusher to coarse chips of 3–5mm in diameter, and then fresh chips without weathered crusts were carefully selected. Subsequently, the chips were rinsed with deionized water in an ultrasonic bath for several times until the supernatants of water became clear. They were then dried up at 100°C for 12h in an oven. The dried chips were pulverized into fine powders using an alumina ceramic puck mill.

S2.1. Major- and trace-element analysis

Concentrations of whole-rock major elements, including Ni and Cr contents, were determined by an X-ray fluorescence spectrometer (Philips PW2400), using glass beads, following the method of Takei (2002). Glass beads were prepared by fusing whole-rock powders (0.500 ± 0.005 g) mixed with anhydrous lithium tetraborate ($Li_2B_4O_7$) in the proportion of 10 to 1 for flux and sample, respectively. The mixture was fused in a platinum crucible using an automated high-frequency bead sampler (Tokyo Kagaku TK-4200). The sample was heated at 1050 ˚C for 10 minutes with continuous stirring and swirling and finally cast into a glass bead. Loss on ignition (LOI) was measured gravimetrically using 0.5–1 g sample. The powdered sample was weighed in the porcelain crucible before and after ignition at 1000 ˚C in a muffle furnace (> 4 hours). All analyses were duplicated and the relative differences among the duplicated analyses were better than 1% for major elements and 5% for Ni and Cr, respectively. Mean abundances of duplicated analyses are summarized in Table S1, and the CIPW normative mineral compositions, calculated from major-element compositions, are summarized in Table S2.

Concentrations of trace elements were determined by an inductively coupled plasma mass spectrometer (ICP-MS) using Agilent 7500cs and Thermo Scientific iCAP TQ following the methods of Yokoyama et al. (1999), Tanaka et al. (2003), Makishima and Nakamura (2006), and Lu et al. (2007). About 20 mg of powdered sample was used, and all analyses were duplicated. Isotope dilution was applied to determination of abundances of B, Zr, Sm, and Hf, and the other elements are determined by internal standardization using elements determined by isotope dilution (isotope-dilution internal standardization method by Makishima & Nakamura, 2006). Analytical reproducibility is better than 3% (as relative standard deviation of replicated analyses of an in-house reference standard rock; see Table S1), except for B (< 5%), Be (< 9%), Cs (< 6%) and Ta (<5%). Mean abundances of duplicated analyses are summarized in Table S1.

S2.2. Sr-Nd-Pb isotope analysis

Isotopic analyses of Sr, Nd, and Pb were performed by thermal ionization mass spectrometers (TIMS) using a Thermo Scientific TRITON and a TRITON plus in a static multi-collection mode. Instrumental mass biases (IBM) during Sr and Nd isotope analyses were corrected using $^{86}Sr/^{88}Sr = 0.1194$ and $^{146}Nd/^{144}Nd = 0.7219$, respectively. The IBM during Pb isotope analysis was corrected by the double-spike method (Kuritani & Nakamura, 2003). Powdered samples (50 mg for Sr-Nd, and 300 mg for Pb) were leached in 6 M HCl at 100°C

for 6 hours prior to acid decomposition to minimize the effect of secondary alteration and contamination. Residues after leaching were rinsed with de-ionized water and decomposed with HF-$HClO_4$ for Sr-Nd isotopes (Yokoyama et al., 1999) and HF-HBr for Pb isotope analyses (Kuritani & Nakamura, 2002). Chemical separations and instrumental procedures followed the methods of Yoshikawa and Nakamura (1993) for Sr, Nakamura et al. (2003) for Nd, and Kuritani and Nakamura (2003) for Pb, respectively. Total procedural blanks for Sr, Nd, and Pb were <260, <7, and <20 pg, respectively. The standard materials during the course of analyses yielded the following means and variants (2σ); $^{87}Sr/^{86}Sr = 0.710276 \pm 0.000008$ ($n = 4$ by TRITON) and 0.710245 ± 0.000008 ($n = 3$ by TRITON plus) for NIST SRM 987, $^{87}Sr/^{86}Sr = 0.703701 \pm 0.000008$ ($n = 2$ by TRITON) and 0.703670 ± 0.000008 ($n = 2$ by TRITON plus) for JB-2; $^{143}Nd/^{144}Nd = 0.511741 \pm 0.000007$ ($n = 6$ by TRITON) and 0.511716 ± 0.000008 ($n = 4$ by TRITON plus) for an in-house standard PML-Nd, those values correspond to $^{143}Nd/^{144}Nd$ of 0.511877 and 0.511852, respectively, for La Jolla (conversion factor of 1.000266 by Makishima et al., 2008), and 0.513119 ± 0.000007 ($n = 2$ by TRITON) and 0.513093 ± 0.000007 ($n = 2$ by TRITON plus) for JB-2; $^{206}Pb/^{204}Pb = 16.9422 \pm 0.0017$, $^{207}Pb/^{204}Pb = 15.4997 \pm 0.0019$, and $^{208}Pb/^{204}Pb = 36.7270 \pm 0.0043$ for NIST SRM 981 ($n = 24$ by TRITON), and $^{206}Pb/^{204}Pb = 18.2956 \pm 0.0013$, $^{207}Pb/^{204}Pb = 15.5375 \pm 0.0014$, and $^{208}Pb/^{204}Pb = 38.2504 \pm 0.0033$ for JB-3 ($n = 5$ by TRITON), respectively. Sample values are reported relative to $^{87}Sr/^{86}Sr = 0.710250$ for NIST SRM 987 and $^{143}Nd/^{144}Nd = 0.511860$ for the La Jolla. The normalization was not applied to Pb-isotopes ratios. Initial $^{87}Sr/^{86}Sr$, $^{143}Nd/^{144}Nd$, $^{206}Pb/^{204}Pb$, $^{207}Pb/^{204}Pb$ and $^{208}Pb/^{204}Pb$ ratios of our samples and those cited from the literature are corrected using the decay constants and atomic ratios of parent nuclides in Steiger & Jäger (1977), and summarized in Table S1.

S2.3. K-Ar dating

Nineteen samples from the mainland and coastal islands were dated by the K-Ar method (Table S3). Samples were crushed to particles of 60–80 mesh (0.18–0.25 mm), and groundmass fractions were collected using a magnetic separator. The abundance of radiogenic ^{40}Ar was determined by an isotope-dilution mass spectrometer, a modified VG5400 mass spectrometer (Micromass, UK), following the method of Nguyen et al. (2020). Instrumental mass bias was corrected using a reference air with $^{40}Ar/^{36}Ar = 296.0$ (Nier, 1950). The abundance of K was determined by a flame photometer AA-

6200 (Shimadzu, Japan). The preparation of samples and instrumental calibration of K analysis are described in Nguyen et al. (2020). All analyses for K and Ar were duplicated. The relative difference of K concentration between duplicates is less than 2%, and the external reproducibility is estimated to be 2% (as $1\sigma_{mean}$) from the repeated analyses of JB-3. The decay constants of ^{40}K via electron capture and β decay follows Steiger & Jäger (1977). During the course of the analyses, the reference standard rocks and minerals (ranging from 1.44 to 17.8 Ma) were analyzed along with samples. Our analyses yielded the ages consistent with those reported in the previous studies (Nagao et al., 1996; Nakamura et al., 1986), thus confirming reliability of the method (Table S4).

Text S3. Petrography

Seventy samples were collected from inland, coastal, and offshore regions in Vietnam. Most samples were fresh, and few samples contained secondary minerals. Major alteration products are iddingsite developed on rims and cracks of olivine, and similar brown products, usually referred to as chlorophaeite or sidenromelane, in interstitial portions of matrices. Carbonates rarely occur in cavities or as olivine pseudomorphs. The petrographic description of representative samples from each region in Vietnam are given below.

S3.1. Con Co Island

All samples from Con Co Island are sub-alkaline basalts and show porphyritic texture (~15 vol%) consisting of phenocrysts of olivine (3–4 vol.%), clinopyroxene (1–2 vol.%) and plagioclase (10 vol.%; Figure S2a). Plagioclase occurs as euhedral shaped crystals (0.5–1 mm). Olivine and clinopyroxene occur as subhedral to anhedral shaped crystals (0.3–0.5 mm). The groundmass mainly consists of olivine, plagioclase, clinopyroxene, and opaque minerals.

S3.2. Ly Son Island and Quang Ngai

Basalts from these regions include alkaline and sub-alkaline types. Alkaline basalts include aphyric type (1–2 vol% phenocryst, PLS23 and PLS35; Figure S2b) and porphyritic type (10 vol% phenocryst, PLS89 and PLS93; Figure S2c). Both types of alkaline basalts have the same phenocryst assemblage consisting of olivine (<6 vol%), clinopyroxene (<3 vol%) and plagioclase (<1 vol%). Olivines occur as euhedral to subhedral shaped crystals (4–6 mm) and are occasionally altered to iddingsite along fractures. The groundmass contains olivine, pyroxene, plagioclase, opaque minerals and minor glass. The sub-alkaline basalts are vesicular and show aphyric texture (<2 vol% phenocryst). Phenocrysts consist of olivine,

clinopyroxene and subordinate plagioclase. Olivine occurs as euhedral shaped crystals (0.5–1 mm). Clinopyroxene occurs as anhedral shaped crystals (0.5 mm). Plagioclase occurs as euhedral to subhedral shaped crystals. Vesicles are occasionally filled by secondary carbonates (PLS36).

S3.3. Kong Plong

A sample MM36 is a sub-alkaline basalt which shows aphyric texture and contains subhedral shaped olivine (< 2 vol.%, 0.3–0.5 mm) as phenocrysts. The groundmass contains olivine, pyroxene, plagioclase and opaque minerals.

S3.4. Pleiku and Buon Ma Thuot

Basalts from this region include alkaline and sub-alkaline series rocks, consistent with Hoàng et al. (2013). Alkaline basalts (KT05; Figure S2d) are aphyric and contain olivine as dominant phenocryst phase (<2 vol%, 0.5 mm). The groundmass of alkaline basalts comprises of olivine, clinopyroxene, plagioclase, opaque minerals and minor glass. Occasionally, they contain large olivines (2.5 mm) with wavy extinction and are considered to be xenocrysts disaggregated from ultramafic xenoliths (Hoàng et al., 2013). Sub-alkaline rocks (KT01, KT02, KT04, KT06; Figure S2d) are phyric to porphyritic (5–6 vol%), containing olivine, clinopyroxene and plagioclase phenocrysts. Porphyritic type contains plagioclase as a major phase with subordinate olivine (KT02). Sample KT04 shows sub-ophitic texture in which plagioclase laths are embedded in subhedral to anhedral shaped clinopyroxenes.

Basalts from Buon Ma Thuot are classified into either alkaline or sub-alkaline, consistent with Hoàng et al. (2013). The alkaline basalts (DK2-2, DK03, DK04, DK05; Figure S2e) show aphyric to phyric texture, consisting of olivine (<5 vol.%) and minor clinopyroxene phenocrysts (<1 vol%). Olivine phenocrysts (1 mm) occur as subhedral to anhedral shaped crystals (DK2-2). Clinopyroxene phenocrysts occur as subhedral shaped crystals (1.5 mm) and have reaction rims of minute opaque minerals (DK03). The groundmass consists of olivine (altered to iddingsite), clinopyroxene, plagioclase, opaque minerals, and minor glass. Vesicular samples contain carbonates as amygdule minerals (DK2-2). Some rocks contain clots of olivine xenocrysts (4 mm) with reaction rims (DK04-05). The sub-alkaline basalts (DK9-1 and DK9-2; Figure S2e) are moderately phyric to porphyritic, containing

phenocrysts of clinopyroxene (<2 vol%, <2 mm), plagioclase (<2 vol%, 1.5 mm) and minor olivine (<1 vol%, <1 mm).

S3.5. Phuoc Long

All studied basalts from Phuoc Long belong to sub-alkaline series. The predominance of this series in this region is reported in Hoang et al. (1996). Basalts show varying texture from aphyric (<2 vol% phenocrysts; DN02 and DN03) to porphyritic (10–20 vol%; DN05, DN08 and DN09; Figure S2f). Phenocryst consists of olivine, clinopyroxene, and plagioclase. Olivine (0.5 mm) occur as major phenocryst phase in both aphyric (< 2 vol%) and porphyritic (<10 vol%) types, and is occasionally altered to iddingsite (DN4-1). Clinopyroxene (<5 vol%) and plagioclase (<15 vol%) occur as common phenocryst phases in porphyritic type (DN05, DN08 and DN09). The groundmass of both types consists of plagioclase, olivine, clinopyroxene, and opaque minerals. Porphyritic type shows sub-ophitic texture in which euhedral shaped plagioclases are embedded in subhedral to anhedral shaped clinopyroxene (DN08).

S3.6. Xuan Loc

Alkaline basalts and sub-alkaline basalts occur in Xuan Loc. They show varying amounts of phenocrysts and exhibit aphyric or porphyritic texture. Alkaline basalts (XL01, XL02, and XL05; Figure S2g) are moderately phyric with phenocrysts of olivine (5–10 vol.%), clinopyroxene (< 2 vol.%), and plagioclase (< 2 vol.%). Olivine is a common phenocryst phase, and occurs as euhedral shaped crystal (1 mm). Xenocryst olivine also occurs, probably disaggregated from ultramafic xenoliths (XL02). Plagioclase occurs as prismatic shaped crystal (<2 mm). Clinopyroxene occurs as subhedral-shaped crystal (0.5 mm; XL05). Orthopyroxene (2 mm, subhedral shape) occasionally occurs in alkaline basalts as a constituent mineral of ultramafic xenoliths (XL02) or disaggregated xenocrysts (XL01). The groundmass consists of plagioclase, clinopyroxene, olivine, opaque minerals and minor glass. Sub-alkaline basalts (XL03 and XL04; Figure S2g) show porphyritic texture with phenocrysts of plagioclase (3–10 vol.%), olivine (5–10 vol.%) and minor clinopyroxene phenocrysts (< 2 vol%). The groundmass consists of plagioclase, pyroxene, olivine, opaque minerals, and minor glass.

S3.7. Phu Quy Island

Basalts from Phu Quy Island include sub-alkaline rocks and alkaline rocks. Irrespective of rock series, basalts in this region show vesicular, aphyric to moderately phyric

texture, and contain phenocrysts consisting of olivine (5–12 vol.%) and minor plagioclase (2–5 vol.%) and clinopyroxene (< 1 vol.%; Figure S2h). Olivine occurs as euhedral to anhedral shaped crystal (1 mm) and is occasionally altered to iddingsite (PQ01 and PQ04-1). Some olivines are replaced by secondary carbonate which also filled in druses (PQ08). Plagioclase occurs as elongate lath-shaped crystal with 1-mm long (PQ02 and PQ06). The groundmass consists of plagioclase, olivine, clinopyroxene, opaque minerals and minor glass.

Text S4. Regional chronology

The K-Ar ages of basaltic rocks by this study (Table S3) are compared with the ages inferred from the stratigraphy (Hoang et al., 1996; Hoang & Flower, 1998; Hoàng et al., 2013) or determined by the K-Ar method or the $^{40}Ar/^{39}Ar$ method in the previous studies (Barr & Macdonald, 1981; Rangin et al., 1995; Lee et al., 1998; Koszowska et al., 2007; An et al., 2017; Le et al., 2019; Hoang et al., 2019).

S4.1. Con Co Island (< 1.3 Ma)

Con Co region in the northernmost part of Central Vietnam includes offshore island (Con Co Island) and onshore areas (Khe Sanh). We analyzed two basalt samples from Con Co Island, yielding the K-Ar ages of 0.06 ± 0.02 and 0.09 ± 0.02 (Figure S3a). These ages are younger than the age of a basalt by the $^{40}Ar/^{39}Ar$ method (0.35 Ma; Lee et al., 1998). The younger ages by this study are possibly due to loss of radiogenic Ar through alteration, although these samples show the effects of intensive alteration (e.g., LOI < 0.1 wt%). Lee et al. (1998) also presented the $^{40}Ar/^{39}Ar$ ages of 1.3 Ma for basalts (n = 2) from the onshore Khe Sanh volcanic field, which is older than the ages of Con Co basalts. The K-Ar ages of 0.44 Ma and 0.55 Ma are also reported for the basalts from the same field by Rangin et al. (1995). Overall, basaltic volcanism in the Con Co region had been active in the Pleistocene.

S4.2. Ly Son Island (<1.2 Ma) and Quang Ngai (7.1–1.5 Ma)

This region includes Ly Son Island (formerly referred to as Re Island) and the coastal area of the mainland at 15.0–15.5 ˚N (Quang Ngai). Two basaltic samples from Ly Son Island yielded K-Ar ages of 0.17 ± 0.02 and 0.03 ± 0.02, and one sample from Quang Ngai yields the K-Ar age of 5.42 ± 0.09 Ma (Figure S3b). The $^{40}Ar/^{39}Ar$ ages of 1.2–0.4 Ma (except for the age of 12 Ma for a basalt) are reported for Ly Son basalts (n = 3) and 7.1–1.5 Ma (n = 2) for Quang Ngai basalts by Lee et al. (1998).

Rangin et al. (1995) reported K-Ar ages of 6.2–1.5 Ma for Quang Ngai basalts (n = 3), demonstrating the consistency of the ages by the K-Ar and $^{40}Ar/^{39}Ar$ methods.

S4.3. Kong Plong (17-10 Ma? and 8–5 Ma)

Basalts occur in the Kong Plong volcanic field of *c*. 2000 km^2, and have volumes of 160 km^3 and thickness of up to 150 m (Hoang et al., 2018; Hoàng et al., 2013; Hoang & Flower, 1998). Eruptions appear to have involved at least two episodes, *c*. 17–10 Ma and 8–7 Ma, based on the stratigraphy of the volcanic field (Hoang et al., 2018). One basaltic sample from this study gave the K-Ar age of 7.55 ± 0.17 Ma (Figure S3c), consistent with the K-Ar ages of 7.0–5.4 Ma (n = 6) by Rangin et al. (1995). The $^{40}Ar/^{39}Ar$ ages have been reported for basalts from the volcanic field.

S4.4. Pleiku (5.4–2 Ma) and Buon Ma Thuot (7.3–0.3 Ma)

Pleiku and Buon Ma Thuot are close to each other, and represent second and third largest volcanic provinces in Vietnam with eruptive volumes of 1500 km^3 and 2000 km^3, respectively (Hoang & Flower, 1998). We did not date basalts in our collection from these provinces since the stratigraphy of these provinces were well established (Hoàng et al., 2013). The $^{40}Ar/^{39}Ar$ ages were reported for basalts from these provinces (Lee et al., 1998); 5.4 to 2.6 Ma for Pleiku and from 7.3 to 0.3 Ma for Buon Ma Thuot (Figures S3d-e). The K-Ar ages were also obtained in the previous studies; 2.1, 1.8 and 1.6 Ma for Pleiku basalts (Barr & Macdonald, 1981; Rangin et al., 1995) and 3.4 Ma for a basalt from Buon Ma Thuot (Barr & Macdonald, 1981).

S4.5. Phuoc Long (15.5 Ma and 8–4.8 Ma)

Phuoc Long is the largest volcanic field in Vietnam straddling the border with Cambodia, with an eruptive volume of 2200 km^3 (Hoang & Flower, 1998). We analyzed one sample from this volcanic field and obtained an age of 6.31 ± 0.58 Ma (Figure S3f). The obtained age falls within the range of the $^{40}Ar/^{39}Ar$ ages (15.5–4.8 Ma) of basalts from this volcanic field (Lee et al., 1998). The older $^{40}Ar/^{39}Ar$ ages (15.5 Ma and 15.1 Ma) by Lee et al. (1998) are obtained for quartz-normative sub-alkaline basalts (Hoang et al., 1996; Hoang & Flower, 1998), and their eruptions seemingly coincided with the cessation of EVS/SCS spreading (15.5–15.1 Ma; Lee et al., 1998). Major volcanic activity had occurred from 8 Ma to 5–4 Ma, dominated by eruptions of olivine-normative basalts and alkaline basalts (Hoang et al., 1996; Hoang & Flower, 1998).

S4.6. Xuan Loc (10 Ma?, 4–2 Ma, and <1 Ma)

Xuan Loc is the southernmost volcanic field in the mainland of Vietnam, and has the eruptive volume of 500 km^3 (Hoang & Flower, 1998). Based on the stratigraphy, Hoang et al. (1996) recognized three phases of Cenozoic volcanism, having occurred at middle Miocene (Phase 1; 10 Ma?), late Pliocene (Phase 2; *c*. 2 Ma), and late Pleistocene (Phase 3; 1 Ma or younger). Radiometric ages and geochemical compositions of Phase-1 volcanic rocks have not been reported. Our samples also do not include Phase-1 volcanic rocks. Four of five basalt samples of this study yielded the K-Ar ages of 1.91–0.53 Ma. These ages are within the range of the $^{40}Ar/^{39}Ar$ ages (2.42–0.24 Ma, $n = 5$) by Lee et al. (1998) and that of the K-Ar ages (2.6–0.2 Ma) by Barr & Macdonald (1981) and Hoang et al. (2019). One of our samples yields a younger K-Ar age of 0.06 ± 0.01 Ma, while An et al. (2017) reported the older K-Ar ages of *c*. 4 Ma. These results indicate that Phase-2 and Phase-3 activities had occurred in 4–2 Ma and 1 Ma to recent (Figure S3g).

S4.7. Phu Quy Island (1.3–0.6 Ma)

Seven basalt samples were dated in this study. The K-Ar ages range from 1.1 to 0.6 Ma (Figure 3h). The older K-Ar ages (2.64 and 1.32 Ma) are reported for basalts from different sites by Le et al. (2019). The older ages are comparable to the $^{40}Ar/^{39}Ar$ age (1.27 Ma) of a basalt from Iles des Cendres island, located at 50-km south of Phu Quy Island (Lee et al., 1998).

S4.8. The other provinces

S4.8.1. Northern Vietnam

Dien Bien Phu is the northernmost volcanic field in Vietnam. The K-Ar and $^{40}Ar/^{39}Ar$ ages of 5.2–4.4 Ma were obtained in the previous studies (Lee et al., 1998; Koszowska et al., 2007). *Phu Quy* or *Nghia Dan* is the volcanic field in Northern Vietnam. A $^{40}Ar/^{39}Ar$ age of 4.5 Ma is reported by Lee et al. (1998).

S.4.8.2. Central Vietnam

Khe Sanh is the volcanic field located in the coastal area of Central Vietnam, and in 50-km west of Con Co Island. The K-Ar and $^{40}Ar/^{39}Ar$ ages of 1.3–0.4 Ma were obtained in the previous studies (Rangin et al., 1995; Lee et al., 1998). *Song Cau* is located in the southeast of Kong Plong, and the basalts from the region yield K-Ar and $^{40}Ar/^{39}Ar$ ages of 10.5–8.9 Ma (Lee et al., 1998; An et al., 2017). Basalts from the

Tuy An region, adjacent to *Song Cau*, yielded K-Ar ages of 7.7 and 7.5 Ma (Rangin et al., 1995).

S.4.8.3. Southern Vietnam

Dalat is the one of the largest basalt plateaus in Vietnam (1500 km^3; Hoang & Flower, 1998). The $^{40}Ar/^{39}Ar$ and K-Ar ages reported in the previous studies range from 14 Ma to 0.2 Ma (Barr & Macdonald, 1981; Rangin et al., 1995; Lee et al., 1998; An et al., 2017).

The *Ile des Cendres* is a group of submarine volcanoes located at 50-km south of Phu Quy Island. The latest activity had occurred during the period from 2 March to 13th May in AD1923 (Patte, 1925). Hoang et al. (1996) and Hoang & Flower (1998) suggested that these volcanoes began active at 2–0.8 Ma.

S.4.8.4. Hainan and Leizhou

The ages of volcanisms in Hainan and Leizhou Peninsula are well constrained by the $^{40}Ar/^{39}Ar$ (and K-Ar) dates, ranging from 12.9 Ma to 0.2 Ma for Hainan and from 1.9 Ma to 0.2 Ma for Leizhou, respectively (Ho et al., 2000; Wang et al., 2012).

S.4.8.5. Laos, Cambodia and Thailand

The ages of Cenozoic basalts in the regions other than Vietnam are reported by Barr & Macdonald (1981), Barr & Cooper (2013 and reference therein), and Sieh et al. (2020 and reference therein), ranging from 24 Ma to 0.1 Ma, and mostly younger than 5 Ma.

Text S5. Geochemistry of basalts from EVS/SCS

Major- and trace-element abundances and $^{87}Sr/^{86}Sr$ and $^{143}Nd/^{144}Nd$ ratios of the sea-floor basalts in EVS/SCS (Site U1431 and Site U1433) were determined (Table S1). The locations of these sites are shown in Figure S4. The abundance patterns of the basalts from Site U1431 and Site U1433 are clearly different. The basalts from Site U1431 have lower abundances of Ba, Th, U, Nb, Ta, and La, compared with the basalts from Site U1433. The overall patterns of normalized element abundances are similar to N-MORB (Gale et al., 2013). The basalts from Site U1433 show the abundances of Rb, Ba, Th, U, Nb, Ta, La and Ce intermediate of N-MORB and E-MORB (Gale et al., 2013). The $^{87}Sr/^{86}Sr$ ratios of the Site-U1431 basalts range from 0.7029 to 0.7032 (Figure S6), which are higher than the average of N-MORB (0.70282 ± 0.00007; Gale et al., 2013). Whereas, the $^{143}Nd/^{144}Nd$ ratios of these basalts show a small variation (0.51298–0.51309), and are comparable to the average of N-MORB (0.51307 ± 0.00002; Gale et al., 2013). In addition, the Site-U1431 basalts show

enrichments of Cs, Rb and K, and depletion of Pb. Such features are considered to have been produced by varying extents of the interaction with seawater (Krolikowska-Ciaglo et al., 2005). Our data are consistent with the data for EVS/SCS basalts from the same and the other sites by Zhang et al. (2018a, 2018b).

Text S6. *F*-test for Pb-isotope correlations

The sums of residual variances (residual sum of squares or RSS) of regression lines in the $(^{206}Pb/^{204}Pb)_i$-$(^{207}Pb/^{204}Pb)_i$ and $(^{206}Pb/^{204}Pb)_i$-$(^{208}Pb/^{204}Pb)_i$ plots are calculated individually for Central and Southern Groups as

$$\mathrm{RSS} = \left[\left(\frac{^{207\text{ or }208}\mathrm{Pb}}{^{204}\mathrm{Pb}}\right)_{\mathrm{observed}} - \left(\frac{^{207\text{ or }208}\mathrm{Pb}}{^{204}\mathrm{Pb}}\right)_{\mathrm{predicted}}\right]^2$$

where subscripts "observed" and "predicted" denotes $^{207}Pb/^{204}Pb$ or $^{208}Pb/^{204}Pb$ determined by the isotopic measurement and predicted by the regression model. The $(^{207\text{ or }208}Pb/^{204}Pb)_{predicted}$ is given as

$$\left(\frac{^{207\text{ or }208}\mathrm{Pb}}{^{204}\mathrm{Pb}}\right)_{\mathrm{predicted}} = b\left(\frac{^{206}\mathrm{Pb}}{^{204}\mathrm{Pb}}\right)_{\mathrm{observed}} + a$$

where $(^{206}Pb/^{204}Pb)_{predicted}$ is $^{206}Pb/^{204}Pb$ determined by the isotopic measurement, and *b* and *a* are slope and intercept of the regression line, respectively (those are given in Table S5). Regression analysis is applied to data for three populations; (1) all samples (i.e., pooled), (2) Central Vietnam samples, and (3) Southern Vietnam samples. The degree of freedom (df) for RSS is $n - 2$ (where n is the number of samples). The combined residual sum of squares ($RSS_{combined}$) is calculated as a sum of RSS for Central Vietnam samples and that for Southern Vietnam samples, and is compared with residual sum of squares for pooled data (RSS_{pooled}). The null hypothesis predicts that statistic *F* given as

$$F = \left(\frac{\mathrm{RSS_{pooled}} - \mathrm{RSS_{combined}}}{\mathrm{df_{pooled}} - \mathrm{df_{combined}}}\right) / \left(\frac{\mathrm{RSS_{combined}}}{\mathrm{df_{combined}}}\right)$$

The *F* should follow the distribution $F(df_{pooled} - df_{combined}, d_{fcombined})$. The $df_{pooled} - df_{combined}$ is 2, and the $d_{fcombined}$ is 34, and the *F* is calculated to be 25.65 and 13.12 for residual variances for regressions of the $^{206}Pb/^{204}Pb$-$^{207}Pb/^{204}Pb$ and $^{206}Pb/^{204}Pb$-$^{208}Pb/^{204}Pb$ relationships, respectively. These *F* are much greater than the predicted *F* [5.29 for $F(2, 34)$ at 1%

significant level and 8.52 for F (2, 34) at 0.1% significant level]. Results are summarized in Table S5.

Text S7. Isotope variability

Isotope variability of basalts in Vietnam and surrounding regions shown in Figure 5 (in the main text) are used to postulate end-member components involved in the magma sources; there are at least four end-member components including D-DMM, EM1 or C1, EM2 or C2, and FOZO. Parameters for the isotope mass-balance mixing model are shown in Table S6. Data sources for the compositions of mantle end-member components are as follows: (1) D-DMM, depleted MORB mantle (Workman & Hart, 2005), $^{208}Pb/^{204}Pb$ of Extreme DM proposed by Salters and Stracke (2004) is substitute for that of D-DMM; (2) EM1/C1 (seamount segment), Sr, Nd and Pb abundances are average of Eastern Wharton Volcanic Province basalts in the northeast Indian Ocean (Hoernle et al., 2011). Proposed isotopic compositions estimated from Pb-Pb systematic and Sr-Nd-Pb systematics; (3) EM2/C2 (sediment), Sr and Nd abundances are average of sediments from Pacific Ocean (Site 1149, Hauff et al., 2003) and Pb abundance adjusted in the compositional range of this Site. Isotope compositions are sediment from Indian Ocean (Ben Othman et al., 1989) which is comparable to sediment from Java trench (Plank & Langmuir, 1998); and (4) FOZO (oceanic crust), trace element abundances are average of altered oceanic Pacific crust (Site 1149, Hauff et al., 2003). Sr-Nd-Pb isotopic compositions are from Stracke et al. (2005).

Text S8. AFC modeling

We examine the extent to which crustal assimilation affects the variations in elemental and isotopic compositions of Vietnamese basalts using the AFC (assimilation and fractional crystallization) model. The Magma Chamber Simulator (MCS) was used for this evaluation, which is a forward modeling tool to examine the evolution of magmatic system based on a thermodynamic model (Bohrson et al., 2014, 2020; Heinonen et al., 2020).

The input parameters include the major- and trace-element compositions and $^{87}Sr/^{86}Sr$-$^{143}Nd/^{144}Nd$ ratios of the parental magmas (PM) and wall rock (WR), temperature changes of the PM and WR during interaction (T interval for simulation), and partition coefficients between minerals and a melt (Table S7). The wall rock compositions were selected from the analyses of the granitic rocks from the Kontum massif (Owada et al., 2007) and Dalat zones (Shellnutt et al., 2013). The enthalpy convergence steps and minimum

wallrock-melt mass fraction follow the suggested ones by Bohrson et al. (2020) and Heinonen et al. (2020).

Text S9. Lithology of basalt magma sources

S9.1. Olivine geochemistry

An et al. (2017) and Hoang et al. (2018) advocated that the sources of Vietnamese basalts contain a significant quantity of mafic crustal lithologies. The argument of the existence of such lithology in the magma sources are based largely on (1) the geochemistry of olivine phenocrysts, and (2) whole-rock major-element compositions. Approach 1 is based on the assumption that magnesian olivine phenocrysts were equilibrated with a parental magma of basalts equilibrated with a mafic or ultramafic source rock. In particular, abundances of minor elements Ca, Mn, Cr, Ni, and Co in olivines are strongly affected by the mineralogy of a source rock. Sobolev et al. (2005, 2007) suggested that melting of an olivine-free mafic lithology (pyroxenites) could produce melts with high-Ni abundance and low-Ca, -Mn and -Cr abundances, compared with melts produced from an olivine-bearing ultramafic lithology (peridotites). A residual solid of mafic lithology should be dominated by pyroxenes and garnet, both of which have lower $D^{solid/melt}$ for Ni and higher $D^{solid/melt}$ for Ca, Mn and Cr, than those of olivine. Accordingly, partitioning of Ni into melt is enhanced while those of Ca, Mn and Cr into melt are suppressed.

An et al. (2017) found that NiO contents of forsteritic olivines (Fo = 85–90) in basalts from Central and Southern Vietnam are as high as 0.37 wt% ([Ni] = 2900 ppm), and fall within the compositional range of olivines in Hawaiian basalts. They suggested that these olivines could have been crystallized from magmas equilibrated with a pyroxenite source. However, the observed NiO range for a given Fo is well within the range of mid-ocean ridge basalts, as clearly shown in Figure 1 in An et al. (2017). Hoang et al. (2018) also found that forsteritic olivines (Fo = 80–90) in basalts from Central Vietnam are depleted in Ca and Mn (hence high Fe/Mn), and again advocated the involvement of pyroxenite sources in production of parental magmas of Vietnamese basalts.

We have compiled major- and minor-element abundance data of olivines (with whole-rock data) by An et al. (2017) and Hoang et al. (2018), and shown in Figure S7. We filtered the olivines with Fo < 88. The Ni abundances (Figure S7a) and those normalized to Fe/Mg abundances (Figure S7b) are well within the range of olivines equilibrated with peridotite-derived melts (Sobolev et al., 2007). The majority of olivine phenocrysts (80%) analyzed by

An et al. (2017) and Hoang et al. (2018) are low-Mg type with Fo < 85, and some of these low-Mg olivines have Ni abundances higher than those estimated by the fractional crystallization model using a constant $D^{olivine/melt}$ for Ni [Figure 2 of Hoang et al. (2018)]. Such olivines are likely equilibrated with melts with low-Mg and high-Si abundances. The experimental studies have documented that $D^{olivine/melt}$ for Ni significantly increases with the increase in SiO_2 abundance and decrease in MgO abundance of a melt (Foley et al., 2013 and reference therein). The low-Ca and low-Mn features of olivine phenocrysts in the Vietnamese could also be explained by changes of $D^{olivine/melt}$ for Ca and Mn under varying pressure condition or vapor fugacity. Using Fe-Mg partitioning (Figure S7c), olivines equilibrated with melts are selected, and $D^{olivine/melt}$ for Ca is estimated for these olivines (Figure S7d). In Figure S7d, the extents to which $D^{olivine/melt}$ varies under varying H_2O and CO_2 are shown by isopleths after Gavrilenko et al. (2016). The observed $D^{olivine/melt}$ for Ca can be explained if a magma contained 0–4 wt% H_2O, consistent with our estimate of H_2O abundances in primary magmas (~2 wt% H_2O). As the CO_2 suppresses $D^{olivine/melt}$ for Ca to a greater extent, the H_2O abundance could be as low as 0–2 wt% to attain the observed $D^{olivine/melt}$.

S9.2. Whole-rock geochemistry

A primary magma was equilibrated with the residual solid of a magma source. It is therefore expected that composition of a primary magmas provides the information about mineral assemblage and melting condition of the source in sub-crustal depth. Basalts emplaced on surface are differentiated to varying extents. The Vietnamese basalt magmas are considered to have been differentiated by crystallization sequence of (1) olivine (+ spinel), (2) olivine (+ spinel) + clinopyroxene, and (3) clinopyroxene ± plagioclase ± olivine ± spinel ± Fe-Ti oxides, based on modal and normative mineral assemblages (Hoang et al., 1996; Hoang & Flower, 1998; this study). The crystallization sequence 2 (cotectic crystallization of olivine and clinopyroxene) is considered to have begun when melt MgO dropped to c. 7.5 wt%, based on the covariation of MgO and CaO/Al_2O_3 of whole-rock samples (Figure S8). At MgO > 7.5 wt%, the basalts in the same volcanic fields and of the same rock series (i.e., alkaline or sub-alkaline series) show nearly constant CaO/Al_2O_3, suggesting crystallization of phases which do not contain significant amounts of CaO or Al_2O_3 (i.e., olivine). Whereas, at MgO < 7.5%, they show a broad positive correlation between MgO and CaO/Al_2O_3, interpreted as participation of clinopyroxene in the assemblage of cotectic phases.

Given that the basalts with MgO > 7.5 wt% are equilibrated with olivine, inverse approach, i.e., incremental addition of equilibrium olivine, can be applied (e.g., Lee et al.,

2009). It is noted that addition of equilibrium olivine does not change CaO/Al_2O_3 (while it increases MgO abundance). The CaO/Al_2O_3 ratio (w/w) of the Vietnamese basalts with MgO > 7.5 wt% ranges from 0.53 to 0.99, being well within the range of partial melts of peridotitic magma sources (Figure S8). Further examination of the magma-source lithology is employed using multiple proxies of major-element oxide components.

It is not straightforward to distinguish melts from peridotite and mafic lithology using a limited number of major-element oxides; in a nominal two-dimensional (2D) plot, the compositions of melts from peridotitic and mafic sources show significant overlaps (Figures S9a and S9b). Yang et al. (2019) developed the algorithm to better characterize multiple-oxide components in 2D representation. They derived multiple proxies by combining major-element oxide components (as logratios); one of the proxies is termed FCKANTMS, that is an acronym for the oxide components used to calculate it (FeO, CaO, K_2O, Al_2O_3, Na_2O, TiO_2, MgO and SiO_2). The FCKANTMS is defined as

$$\begin{aligned}\mathrm{FCKANTMS} = {} & \ln\left(\frac{\mathrm{FeO}}{\mathrm{CaO}}\right) \\ & - 0.08\ln\left(\frac{\mathrm{K_2O}}{\mathrm{Al_2O_3}}\right) \\ & - 0.052\ln\left(\frac{\mathrm{TiO_2}}{\mathrm{Na_2O}}\right) \\ & - 0.036\ln\left(\frac{\mathrm{Na_2O}}{\mathrm{K_2O}}\right)\ln\left(\frac{\mathrm{Na_2O}}{\mathrm{TiO_2}}\right) - 0.062\left[\ln\left(\frac{\mathrm{MgO}}{\mathrm{SiO_2}}\right)\right]^3 - 0.641\left[\ln\left(\frac{\mathrm{MgO}}{\mathrm{SiO_2}}\right)\right]^2 \\ & - 1.871\ln\left(\frac{\mathrm{MgO}}{\mathrm{SiO_2}}\right)^3 - 1.473\end{aligned}$$

where all the oxide abundances are in wt%. The coefficients for major-element logratios in the above equation are optimized so as to adjust the mean FCKANTMS value for the melts from 'pyrolitic' lherzolite (KR4003; Walter, 1998) to be 0 (± 0.08 as 1σ).

Yang et al. (2019) found that FCKANTMS values of the experimental melts from mafic lithologies (pyroxenites; Hirschmann et al., 2003; Keshav et al., 2004; Kogiso et al., 2003; Lambart et al., 2009b; Lambart et al., 2013; Figure S9c) is much greater than 0. Also, they found that the existence of CO_2 enhances the differences in FCKANTMS values from melts from these two different lithologies. The melts of CO_2-bearing peridotites (Dasgupta et al., 2007) yield extremely low FCKANTMS values (as low as –2), whereas the melts of CO_2-

bearing eclogites (Dasgupta et al., 2006) yield extremely high FCKANTMS values (as low as +2).

It is well known that mafic lithology includes silica-deficient type and silica-excess type (e.g., Kogiso et al., 2003). Silica-deficient mafic rocks have mineralogic and major-element characteristics between silica-excess mafic rocks and peridotites (e.g., Yaxley & Green, 1998). Yang et al. (2019) demonstrated that melts from silica-deficient rocks also show FCKANTMS values intermediate between silica-excess mafic rocks and peridotites (thus they denoted this compositional range as "transitional lithology"). Accordingly, they gave two thresh values which discriminate (silica-excess) mafic lithology, transitional lithology, and peridotite; 0.37 ± 0.08 for a boundary of mafic lithology and transitional lithology, and 0.05 ± 0.10 for a boundary of silica-deficient mafic lithology and peridotite (Figure S9c).

It is noted that FCKANTMS is little affected by crystallization of olivine (Yang et al., 2019), hence it is applicable to samples with liquidus phases of merely olivine (with minor spinel). We have calculated the FCKANTMS values for the Vietnamese basalts (data by this study and the existing data for basalts with MgO > 8 wt%), and plotted against $Mg^{\#}$ in Figure S9c. The Vietnamese basalts have the FCKANTMS values of –0.04–0.50 (a mean of 0.27 ± 0.11, 1σ) irrespective of $Mg^{\#}$, which are well within the fields of melts from peridotite and transitional lithology. We thus conclude that "olivine-free" lithology did not largely contribute to the formation of primary magmas of the Vietnamese basalts.

Text S10. H_2O and CO_2 abundances in parental magmas of Vietnamese basalts

We employed thermobarometry to examine the pressure and temperature conditions of magma production. The existing thermobarometers are used (Putirka et al., 2008; Lee et al., 2009; Herzberg & Asimow, 2015; Plank & Forsyth, 2016), which are calibrated using the experimental data on melting of ultramafic lithologies (peridotite). These studies demonstrated that melting under varying pressure and temperature conditions produced magmas with different compositions. It is also noted that volatiles (H_2O and CO_2) significantly affect melting behavior (reaction stoichiometry, solidus depression/elevation) and major-element compositions of partial melts (e.g., Hirose, 1997; Dasgupta et al., 2007). In applying thermobarometry, it is essential to evaluate H_2O and CO_2 abundances in parental magmas of Vietnamese basalts.

The H_2O is incompatible with major mineral phases considered to have been crystallized from parental magmas of Vietnamese basalts (olivine, pyroxene, feldspar and Fe-Ti oxides). The partition coefficients of H_2O between a magma and these minerals are considered to be similar to light rare-earth elements such as Ce; bulk partition coefficient of H_2O (and Ce) is as small as 0.01 (Michael, 1995; Danyuschevsky et al., 2000). Thus, the H_2O/Ce ratio of a primary magma is essentially identical to its magma source. Dixon et al. (2002) gave the estimates of H_2O/Ce ratios in mantle end-member components (DMM, FOZO, and EM) of 100–250. Cabral et al. (2014) also demonstrated that the larger number of the data for MORB and OIB cluster chiefly in the range of H_2O/Ce ratio 200 ± 50. We estimated H_2O abundance in primary magmas of Vietnamese basalts using the constant H_2O/Ce ratio of 200, and Ce abundance of the primary magmas estimated by incremental addition of equilibrium olivine ($D_{\mathrm{Ce}}^{\mathrm{olivine/melt}} = 0.0005$; McKenzie & O'Nions, 1991).

The CO_2 (or C) is also incompatible with major mineral phases in Vietnamese basalts. Hirschmann (2018) demonstrated that CO_2/Ba ratios of MORB and OIB cluster chiefly in the interval 100 ± 20. He also found a smaller variation in CO_2/Nb ratios (810 ± 220) of these oceanic basalts. These ratios are multiplied with Ba or Nb abundances in calculated primary magmas, and the abundance of CO_2 was estimated as.

$$\mathrm{CO_2\ (wt\%)} = 100\ (\pm\ 20) \times\ \mathrm{Ba\ (\mu g \cdot g^{-1})} \times 10^{-4}$$

and

$$\mathrm{CO_2\ (wt\%)} = 810\ (\pm\ 220) \times\ \mathrm{Nb\ (\mu g \cdot g^{-1})} \times 10^{-4}.$$

It is noted that Ba and Nb abundances in the above equations are those in a primary magma, calculated using $D_{\mathrm{Ba}}^{\mathrm{olivine/melt}} = 1.3 \times\ 10^{-6}$ (Beattie, 1994) and $D_{\mathrm{Nb}}^{\mathrm{olivine/melt}} = 0.01$ (McKenzie & O'Nions, 1991), respectively.

Dasgupta et al. (2007, 2013) experimentally documented the composition of partial melts from CO_2-bearing peridotites. The most striking feature is that CO_2 diminishes SiO_2 in melts, resulting in the linear relationship between SiO_2 and CO_2 abundances in melts. Plank & Forsyth (2016) and obtained the following relationship from the experimental data by Dasgupta et al. (2007, 2013) as

$$\mathrm{SiO_2\ (wt\%)} = -1.067 \times \mathrm{CO_2\ (wt\%)} + 50.63.$$

560 It is noted that the above equation is applicable to melts formed at 2–3 GPa. In Figure S10,
561 the CO_2 abundances estimated from the abundances of Ba ($[CO_2]_{Ba}$), Nb ($[CO_2]_{Nb}$), and SiO_2
562 ($[CO_2]_{Si}$) are shown. The $[CO_2]$ estimates among the different approaches agree with each
563 other within ± 0.7 wt% uncertainty.

564 **Text S11. The condition of melting: major-element and trace-element approaches**

565 Melting pressure and temperature, calculated by thermobarometers (Putirka, 2008;
566 Lee et al., 2009; Herzberg & Asimow, 2015 Plank & Forsyth, 2016) are summarized in Table
567 S8 and shown in Figure S11. Mantle potential temperatures are calculated by the algorithm of
568 Plank & Forsyth (2016) or the adiabatic gradient by Katz et al. (2013), and the results are
569 shown in Figure S12. The parameters used REE modeling (REEBOX PRO; Brown & Lesher,
570 2016) is summarized in Table S9.

571

572 **Figures S1 to S12**

573

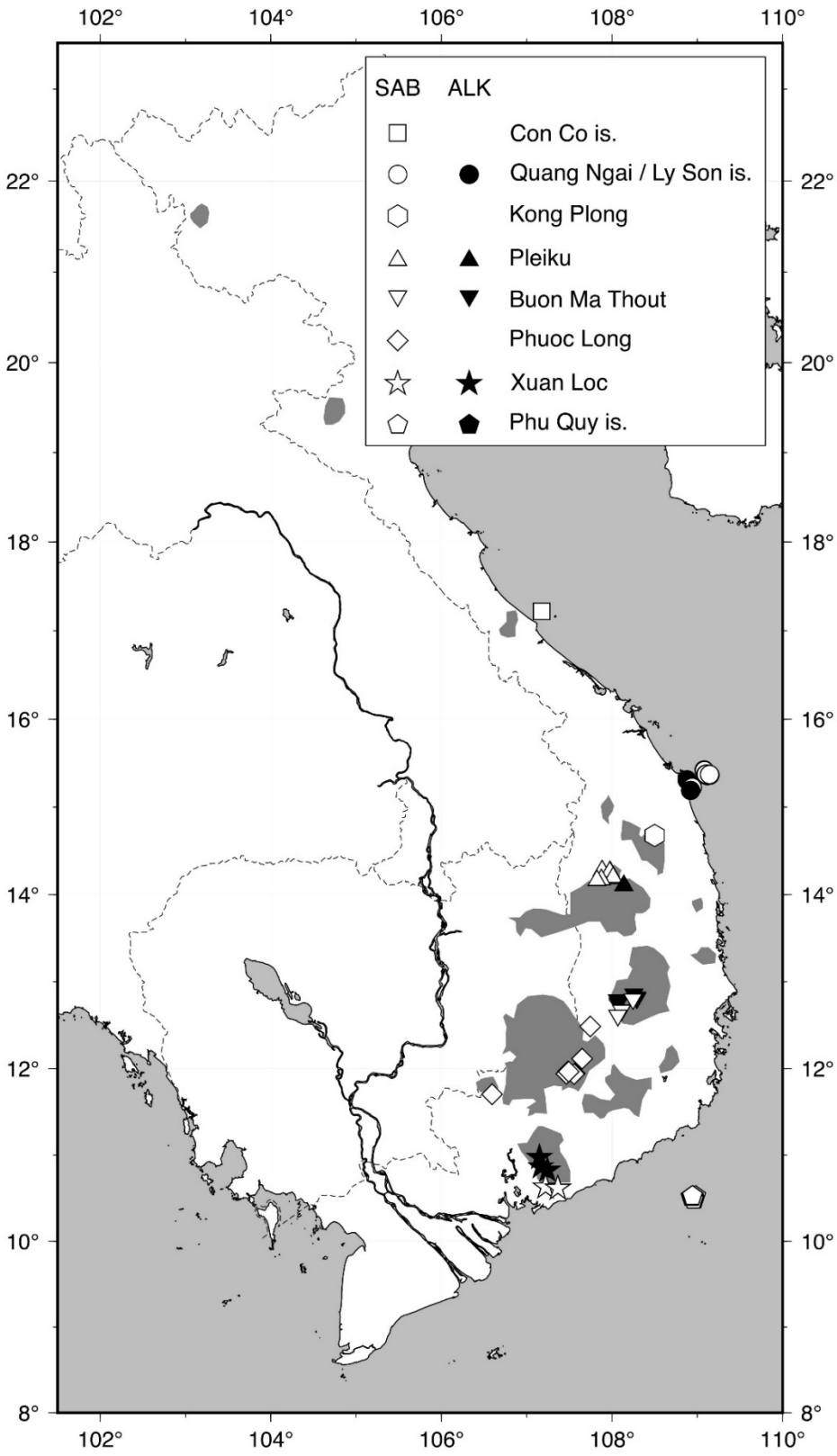

Figure S1: Map showing sample localities. Open symbols, sub-alkaline basalts (SAB), filled symbols, alkaline basalts (ALK). Gray fields denote distributions of basaltic lava flows in Vietnam (Hoang et al., 1996).

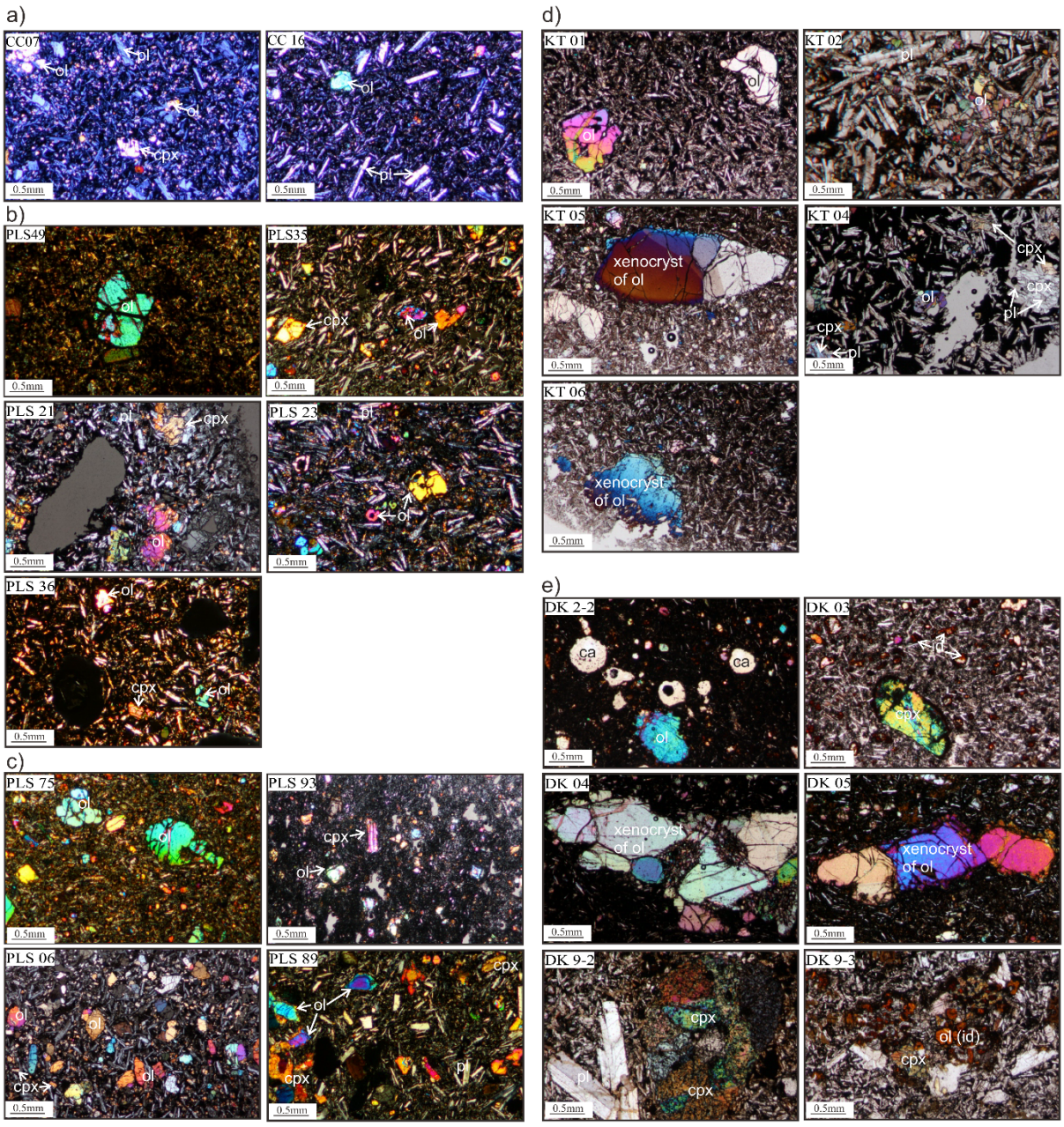
a)
CC07
ol
ol
pl
ol
cpx
0.5mm
CC 16
ol
pl
0.5mm
b)
PLS49
ol
0.5mm
PLS35
cpx
ol
0.5mm
PLS 21
pl
cpx
ol
0.5mm
PLS 23
pl
ol
0.5mm
PLS 36
ol
cpx
ol
0.5mm
c)
PLS 75
ol
ol
0.5mm
PLS 93
cpx
ol
0.5mm
PLS 06
ol
ol
ol
cpx
0.5mm
PLS 89
cpx
ol
cpx
pl
0.5mm
d)
KT 01
ol
ol
0.5mm
KT 02
pl
ol
0.5mm
KT 05
xenocryst of ol
0.5mm
KT 04
cpx
ol
cpx
pl
cpx
ol
0.5mm
KT 06
xenocryst of ol
0.5mm
e)
DK 2-2
ca
ca
ol
0.5mm
DK 03
pl
cpx
0.5mm
DK 04
xenocryst of ol
0.5mm
DK 05
xenocryst of ol
0.5mm
DK 9-2
cpx
pl
cpx
0.5mm
DK 9-3
ol (id)
cpx
0.5mm

579

580

581

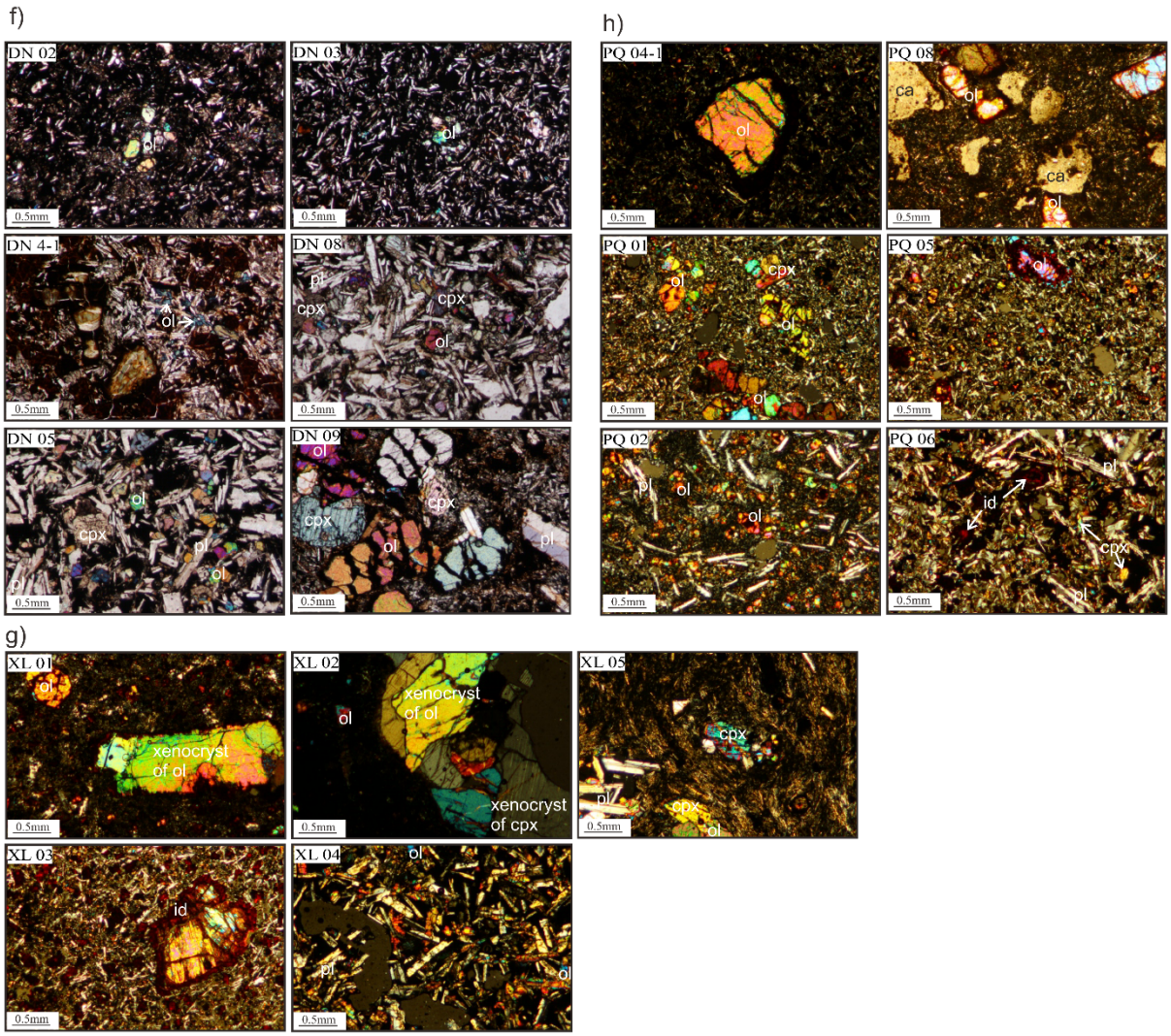

Figure S2: Photomicrographs of (a) sub-alkaline basalts from Con Co Island (CC07 and CC16) with porphyritic texture containing phenocrysts of olivine (ol), plagioclase (pl) and clinopyroxene (cpx), (b) alkaline basalts from Ly Son-Quang Ngai region showing aphyric (PLS75, PLS93) to porphyritic textures (PLS06, PLS89) and containing ol, cpx and pl as phenocrysts, (c) sub-alkaline basalts from Ly Son-Quang Ngai region with aphyric (PLS49) to porphyritic (PLS21, PLS23, PLS35, PLS36) textures containing ol, pl and cpx as phenocrysts, (d) alkaline (KT05) and sub-alkaline basalts (KT01, KT02, KT04 and KT06) from Pleiku with aphyric (KT01, KT05, KT06) to porphyritic (KT02) textures or sub-ophitic texture (KT04) in which pl lath is embedded in cpx, (e) alkaline (DK2-2, DK03, DK04, DK05) and sub-alkaline (DK9-2 and DK9-3) basalts from Buon Ma Thuot with aphyric texture (DK2-2, DK03, DK04, DK05), carbonates (ca) as ol (or iddingsite, id) pseudomorphs (DK2-2), olivine xenocryst (DK04 and DK05), and porphyritic texture (DK9-2 and DK9-3), (f) sub-alkaline basalts (aphyric type, DN02 and DN03; moderately-phyric type, DN4-1; porphyritic type, DN05, DN08, and DN09) from Phuoc Long with phenocrysts of ol, cpx and

pl, (g) alkaline basalts (XL01, XL02, and XL05) with aphyric to phyric texture and sub-alkaline basalts (XL03 and XL04) with porphyritic texture from Xuan Loc, and (h) alkaline basalt (PQ05) with aphyric texture and ol phenocryst and sub-alkaline basalts (PQ01, PQ02, PQ04-1, PQ06 and PQ08) with moderately phyric textures and phenocrysts of ol, pl and cpx from Phu Quy Island.

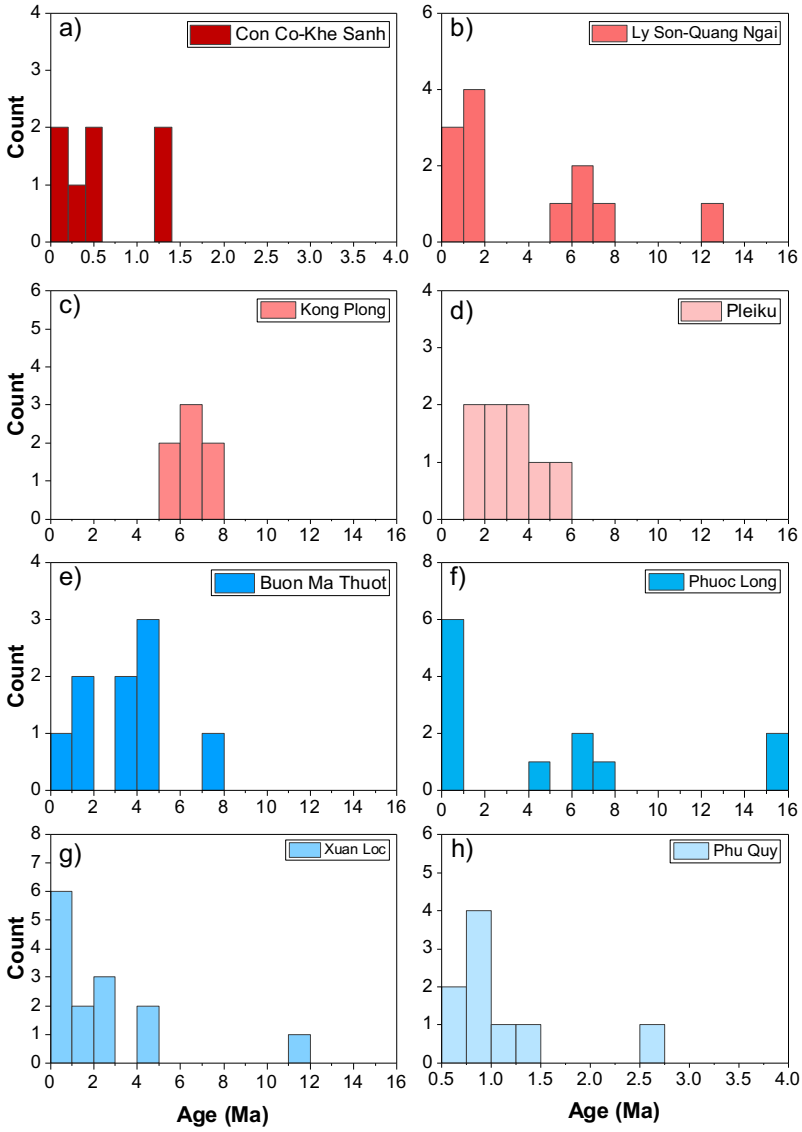

603

604 **Figure S3:** Histogram showing variations in age of Vietnamese basalts in each volcanic field.
605 The data are from this study (Table S3) and literature (An et al., 2017; Barr & Macdonald,
606 1981; Hoang et al., 2019; Le et al., (2019); Lee et al., 1998; Rangin et al., 1995).

607

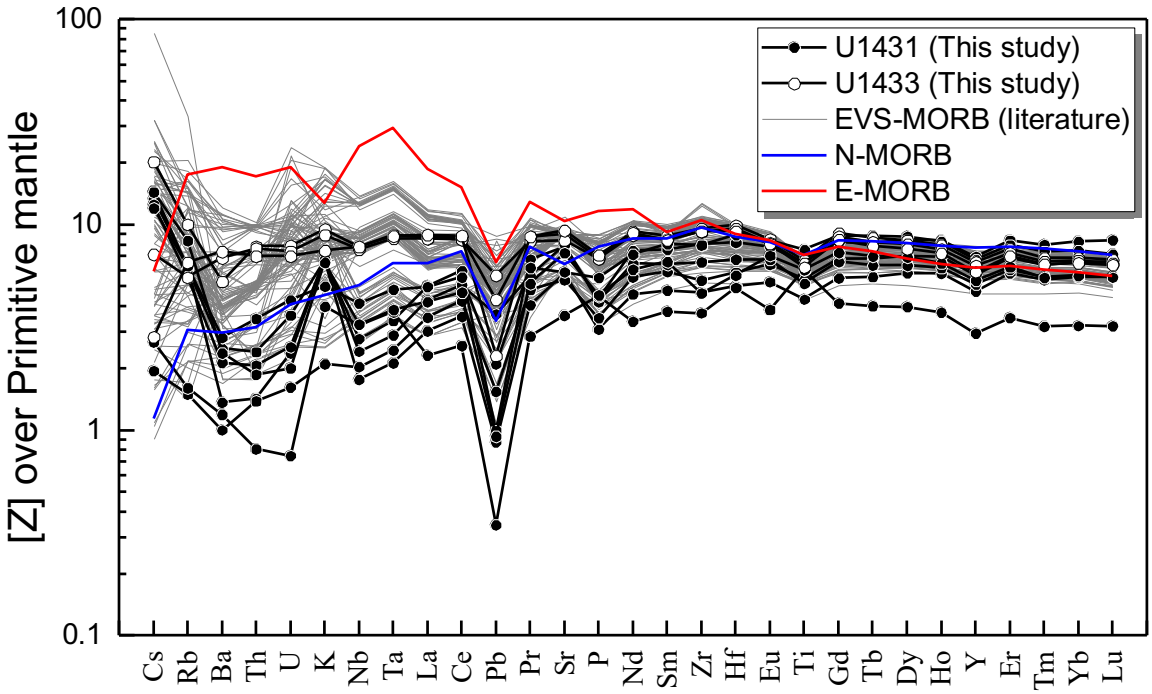

608

609 **Figure S4:** Primitive mantle-normalized trace-element abundance patterns of seafloor basalts
610 from the EVS/SCS (Sites U1431 and U1433, this study; literature data for basalts from these
611 and the other sites are from Zhang et al. (2018a, 2018b)). Abundances of trace elements in N-
612 MORB and E-MORB are from Gale et al. (2013). Abundance of trace elements in primitive
613 mantle are from McDonough and Sun (1995).
614

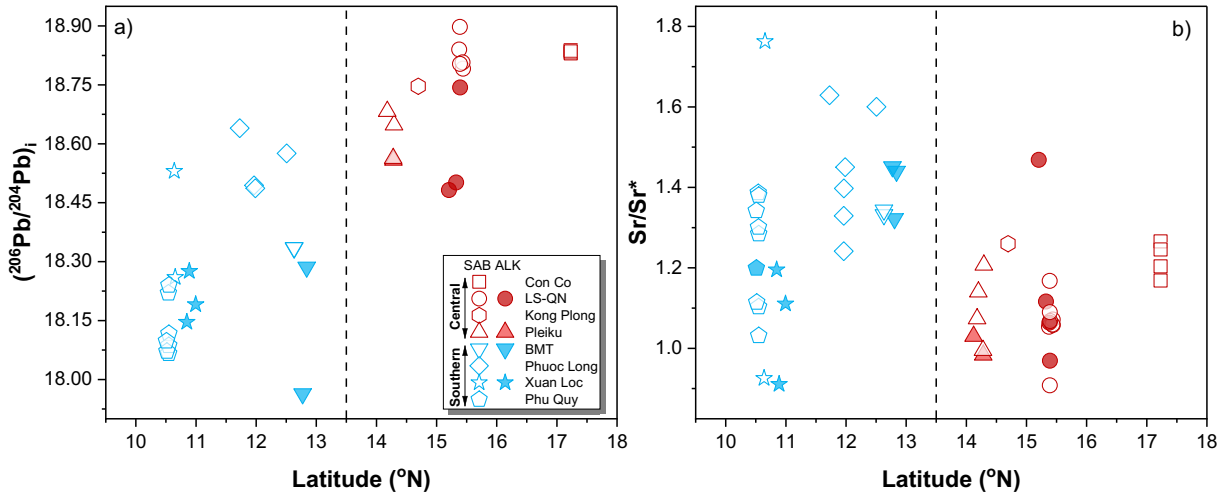

615

616

617 **Figure S5:** (a) $(^{206}Pb/^{204}Pb)_i$ versus Latitude and (b) Sr/Sr* versus Latitude.
618 $Sr/Sr^* = Sr_N/(Ce_N \times Nd_N)^{0.5}$, where the subscript *N* indicates normalization to primitive
619 mantle (McDonough & Sun, 1995).

620

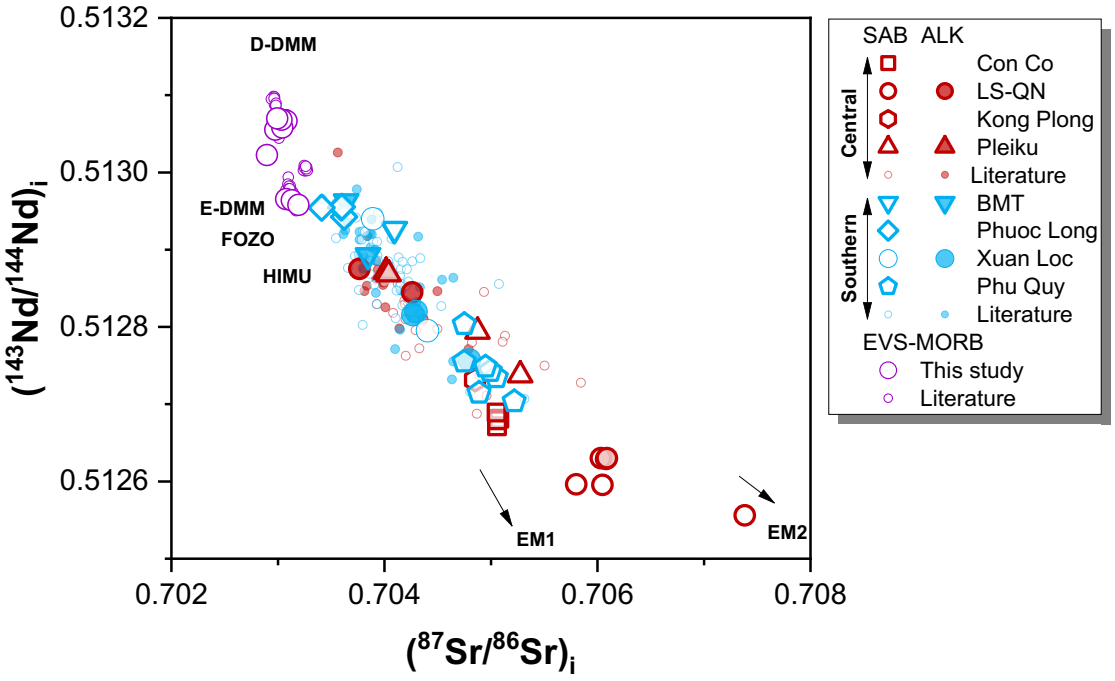

Figure S6: Sr-Nd isotopic compositions of late Cenozoic mafic volcanic rocks from Vietnam and the EVS compared with literature data (An et al., 2017; Hoang et al., 2018; Hoàng et al., 2013; Hoang et al., 1996, 2019; Zhang et al., 2018a, b). Data sources for the compositions of mantle end-member components are as follows: D-DMM and E-DMM, Workman and Hart (2005); EM1 and EM2, Zindler and Hart (1986); HIMU and FOZO, Stracke et al. (2005). Analytical uncertainties of our data are smaller than the symbols. Isotopic ratios are age-corrected (denoted as subscript i; Table S1). ALK and SAB indicate alkaline and sub-alkaline basalts, respectively.

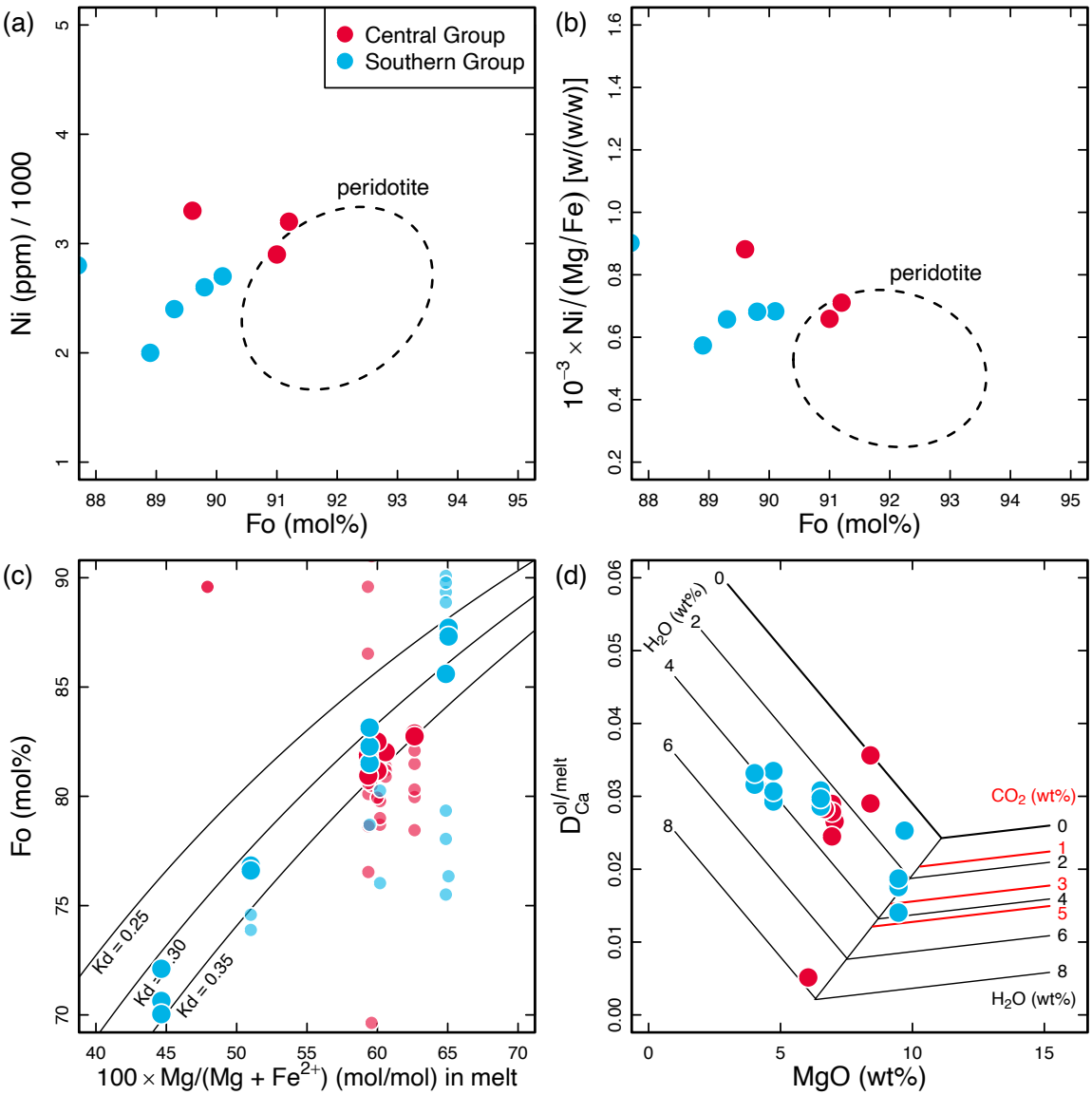

Figure S7: The geochemistry of olivine phenocrysts in basalts from Central and Southern Vietnam: (a) Fo [≡ 100 × Mg/(Mg + Fe^{2+}) in molar] vs. Ni abundances; (b) Fo vs. Ni abundances normalized by Mg/Fe weight (w) ratio; (c) Fo compared with 100 × Mg/(Mg + Fe^{2+}) (in molar) of melt (i.e., bulk); (d) Ca abundance (relative to bulk, i.e., partitioning, expressed as $D_{Ca}^{ol/melt}$) vs. MgO (wt%) of melt. The circles drawn by broken line in (a) and (b) denote the compositions of olivine equilibrated with primary magmas produced by melting of peridotites (Sobolev et al., 2007). The lines denoted as Kd = 0.25, 0.30, and 0.35 are the Fo of olivines equilibrated with melt [where Kd = $(Fe^{2+}/Mg)_{olivine}/(Fe^{2+}/Mg)_{melt}$] (Roeder & Emslie, 1970; Blundy et al., 2020). Data fall between the lines of Kd = 0.25 and Kd = 0.35 are shown as larger symbols. The black and red lines in (d) denote $D_{Ca}^{ol/melt}$ for varying amount of H_2O and CO_2 in melts (i.e., isopleths of H_2O and CO_2) after Gavrilenko et al. (2016). Data plotted in (d) are those for olivines having Kd = 0.25–0.35.

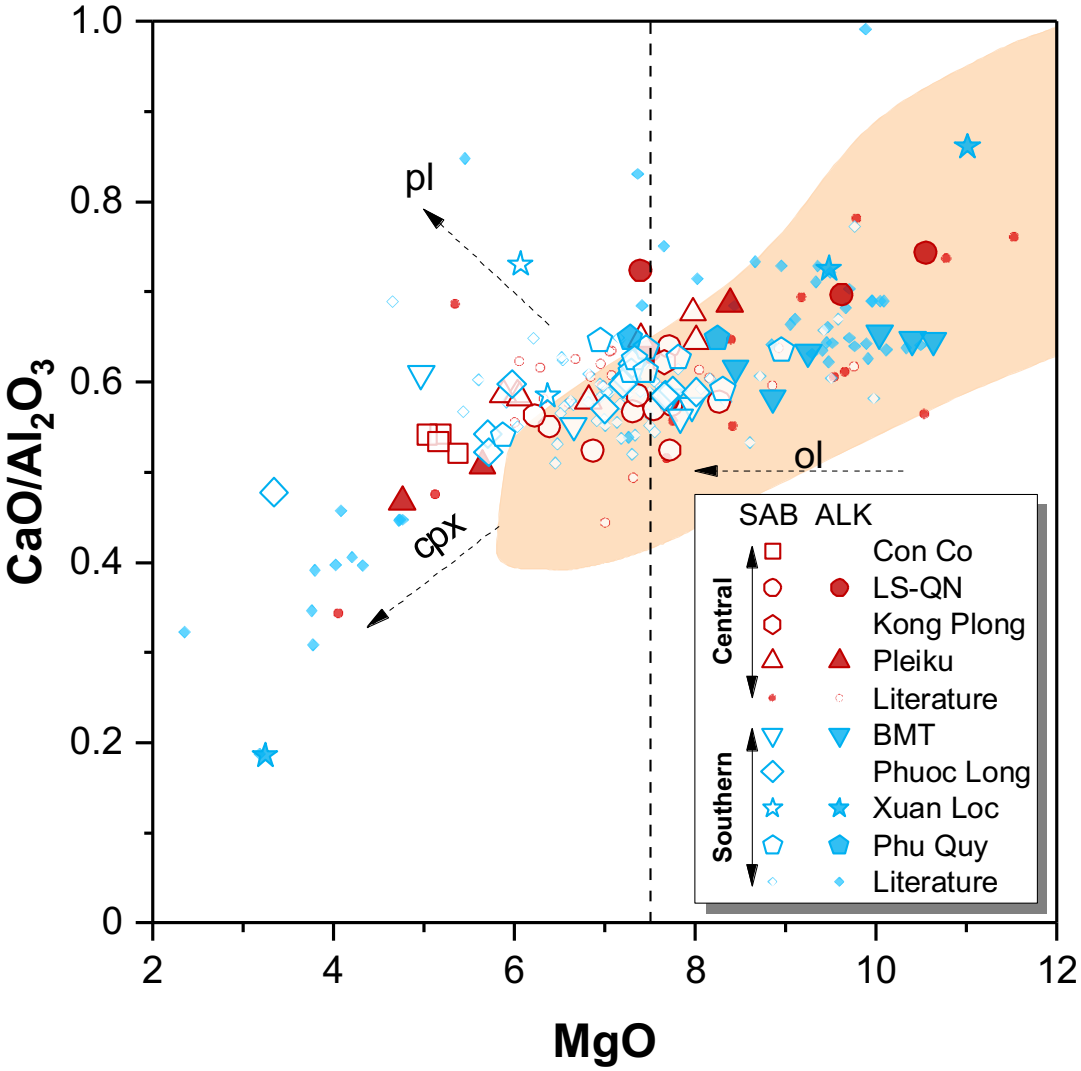

Figure S8: Plot of MgO versus CaO/Al_2O_3 for Vietnamese basalts from this study and literature (An et al., 2017; Hoàng et al., 2013; Hoang et al., 1996, 2019; Hoang et al., 2018). Data sources for experimental peridotite melts (orange field; Condamine et al., 2016; Davis et al., 2011; Davis & Hirschmann, 2013; Falloon & Danyushevsky, 2000; Hirose & Kawamura, 1994; Hirose & Kushiro, 1993, 1998; Kushiro, 1996; Pickering-Witter & Johnston, 2000; Walter, 1998) are shown for comparison. The vectors denoted as "ol", "pl", and "cpx" depict compositional changes by fractionation of olivine, plagioclase, and clinopyroxene, respectively.

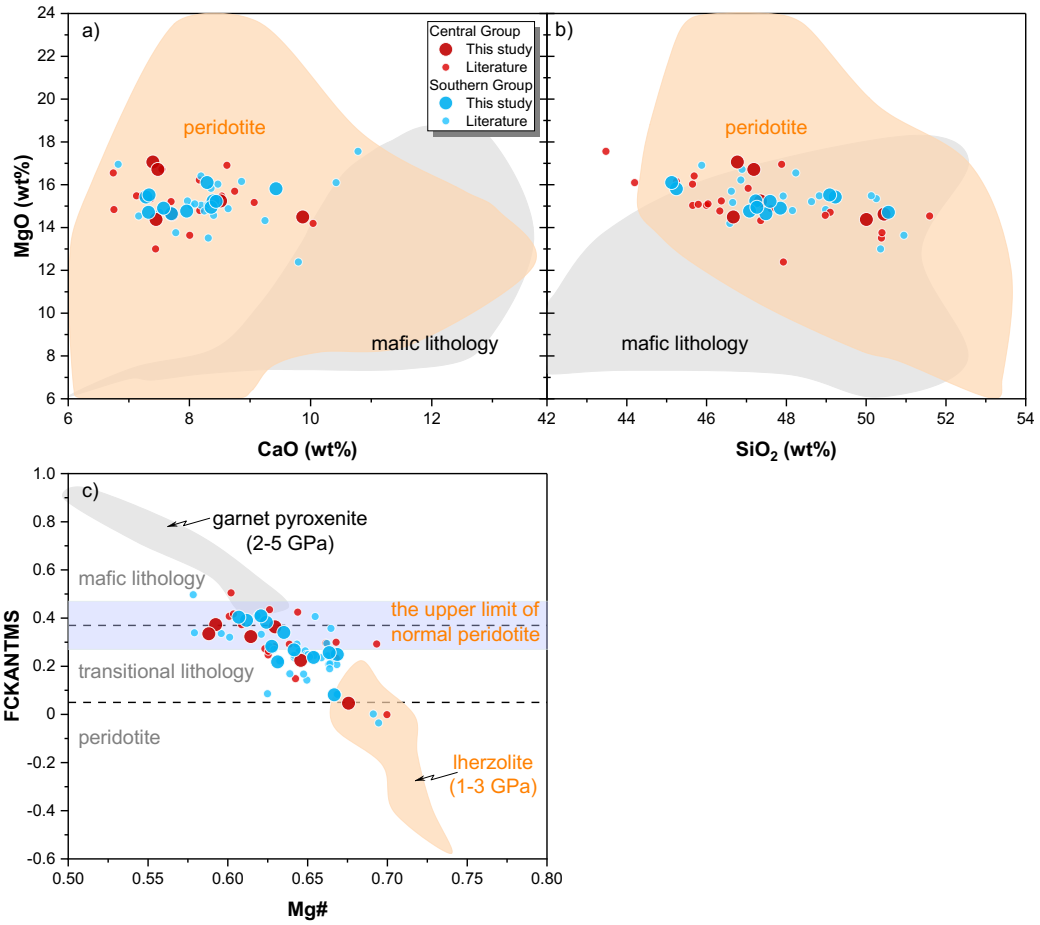

Figure S9: (a, b) Plot of MgO versus CaO, and MgO versus SiO_2 for calculated primary magmas of Vietnamese basalts. Data for basalts in Central and Southern Vietnam are from this study and the previous studies (An et al., 2017; Hoàng et al., 2013; Hoang et al., 1996, 2019; Hoang et al., 2018). Compositions of experimental melts of anhydrous peridotite (Condamine et al., 2016; Davis et al., 2011; Davis & Hirschmann, 2013; Falloon & Danyushevsky, 2000; Hirose & Kawamura, 1994; Hirose & Kushiro, 1993, 1998; Kushiro, 1996; Pickering-Witter & Johnston, 2000; Walter, 1998), and those of mafic lithologies (eclogite, pyroxenite; Hirschmann et al., 2003; Keshav et al., 2004; Kogiso et al., 2003; Lambart et al., 2009a, 2012) are also shown for comparison. (c) FCKANTMS versus Mg# [$\equiv$ $Mg/(Mg + Fe^{2+})$ in molar] for Vietnamese basalts with MgO > 8 wt%. The parameter FCKANTMS is defined by Yang et al. (2019) as; $\ln(FeO/CaO) - 0.08 \times \ln(K_2O/Al_2O_3) - 0.052 \times \ln(TiO_2/Na_2O) - 0.036 \times \ln(Na_2O/K_2O) \times \ln(Na_2O/TiO_2) - 0.062 \times [\ln(MgO/SiO_2)]^3 - 0.641 \times [\ln(MgO/SiO_2)]^2 - 1.871 \times \ln(MgO/SiO_2) - 1.473$, where all oxides are in wt %. Two dashed lines separate the compositions of melts from mafic lithology, transitional lithology and peridotite (FCKANTMS at 0.37 ± 0.08 and 0.05 ± 0.10). The border of mafic lithology and transitional lithology is denoted as "the upper limit of melts of normal peridotite" by Yang et al. (2019). Experimental melts of garnet pyroxenites (2–5 GPa) are from Hirschmann et al. (2003), Keshav et al. (2004), Kogiso et al. (2003), Lambart et al. (2009b), and Lambart et al. (2013). Experimental melts of lherzolite mineralogies (1–3 GPa) are from Davis et al. (2011) and Davis & Hirschmann (2013).

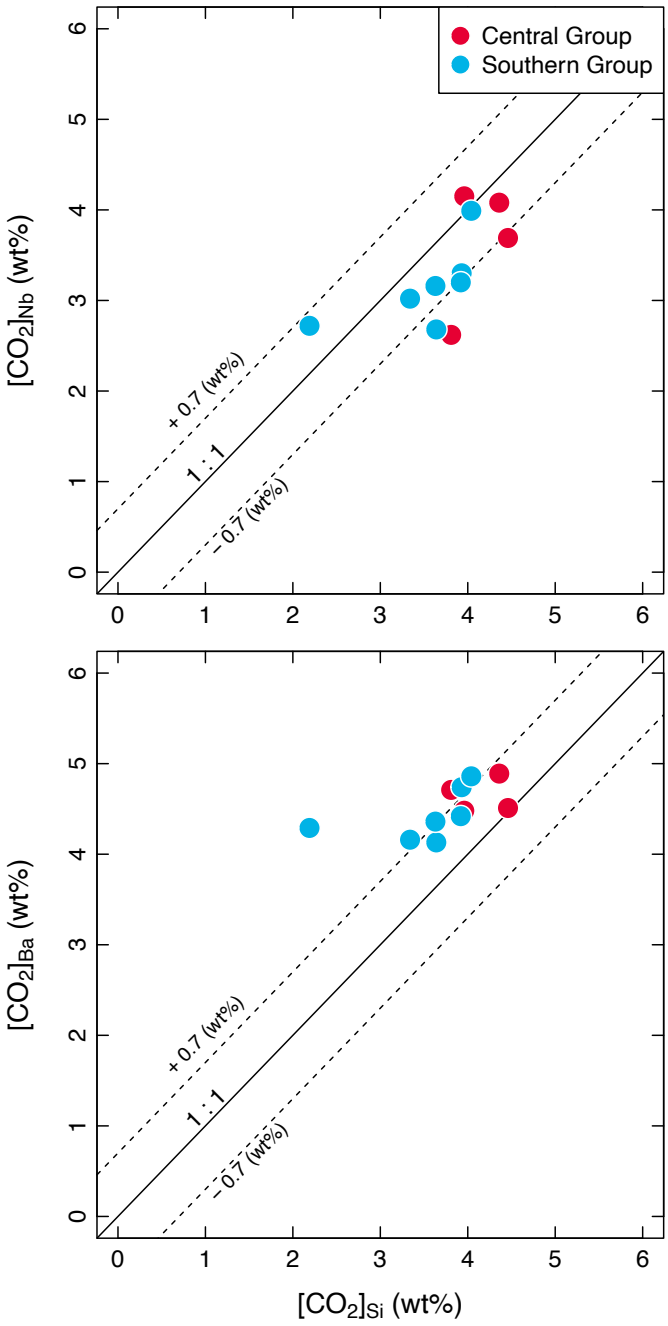

681

682 **Figure S10:** Comparison of CO_2 abundance in the primary magmas of the Vietnamese
683 basalts estimated from SiO_2 abundance ($[CO_2]_{Si}$ following Plank & Forsyth, 2016), Nb
684 abundance ($[CO_2]_{Nb}$, following Hirschmann, 2018) and Ba abundance ($[CO_2]_{Ba}$, following
685 Hirschmann, 2018) in the primary magmas calculated by incremental addition of equilibrium
686 olivine (Lee et al., 2009).
687

688

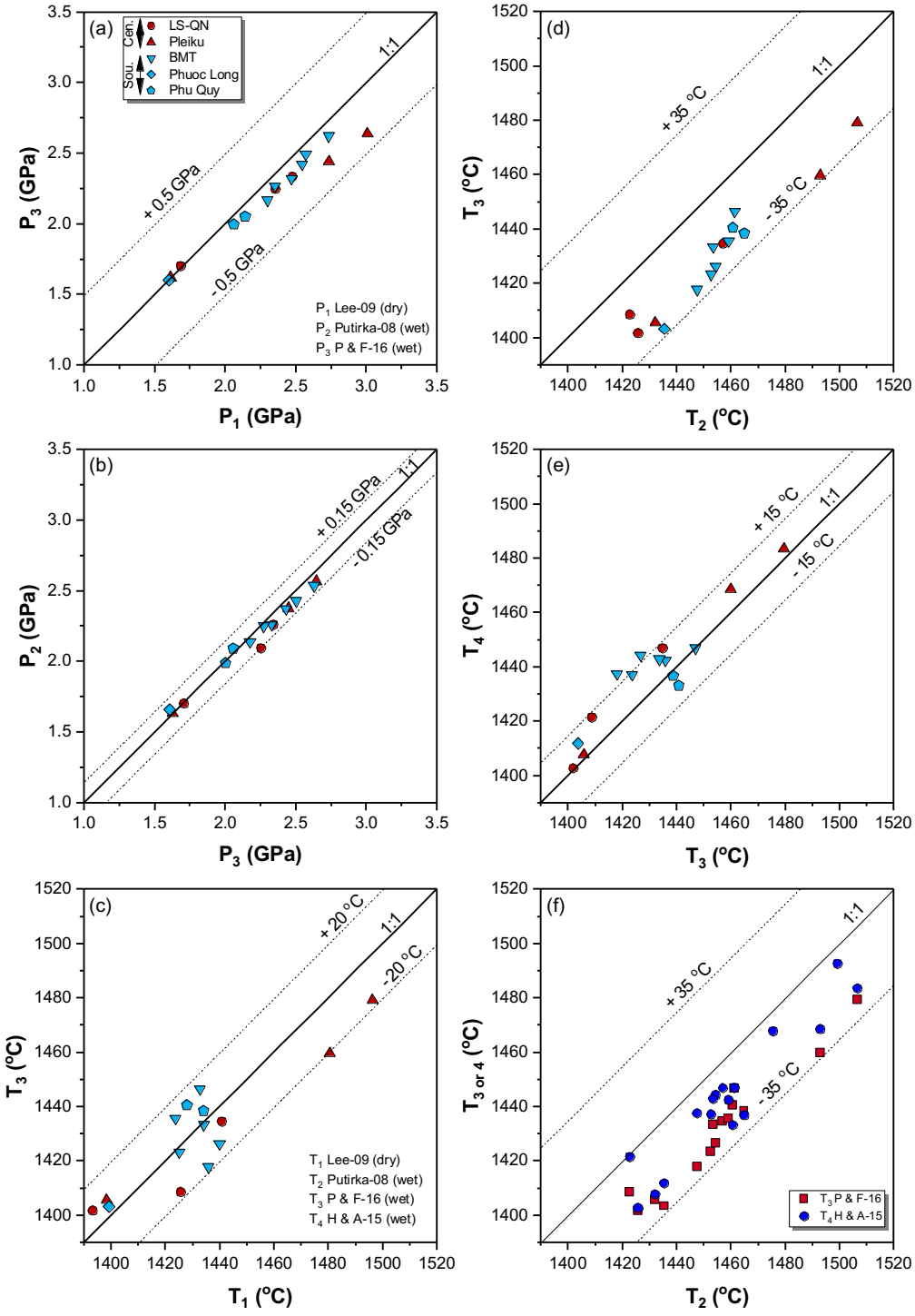

Figure S11: Results of thermobarometry for Vietnamese basalts (MgO > 8.0 wt %). Melting temperature (T) and pressure (P) under anhydrous condition are estimated using the methods of Lee et al. (2009) (P_1 and T_1), and under hydrous condition ($H_2O \pm CO_2$) using the models of Putirka (2008) (P_2 and T_2), Plank and Forsyth (2016) (P_3 and T_3) and Herzberg and Asimow (2015) (T_4). Estimated H_2O and CO_2 contents in melts are 0.47–2.0 wt% and 2.2–4.5 wt%, respectively. Symbols are arranged in latitude from north (LS-QN) to south (Phu Quy).

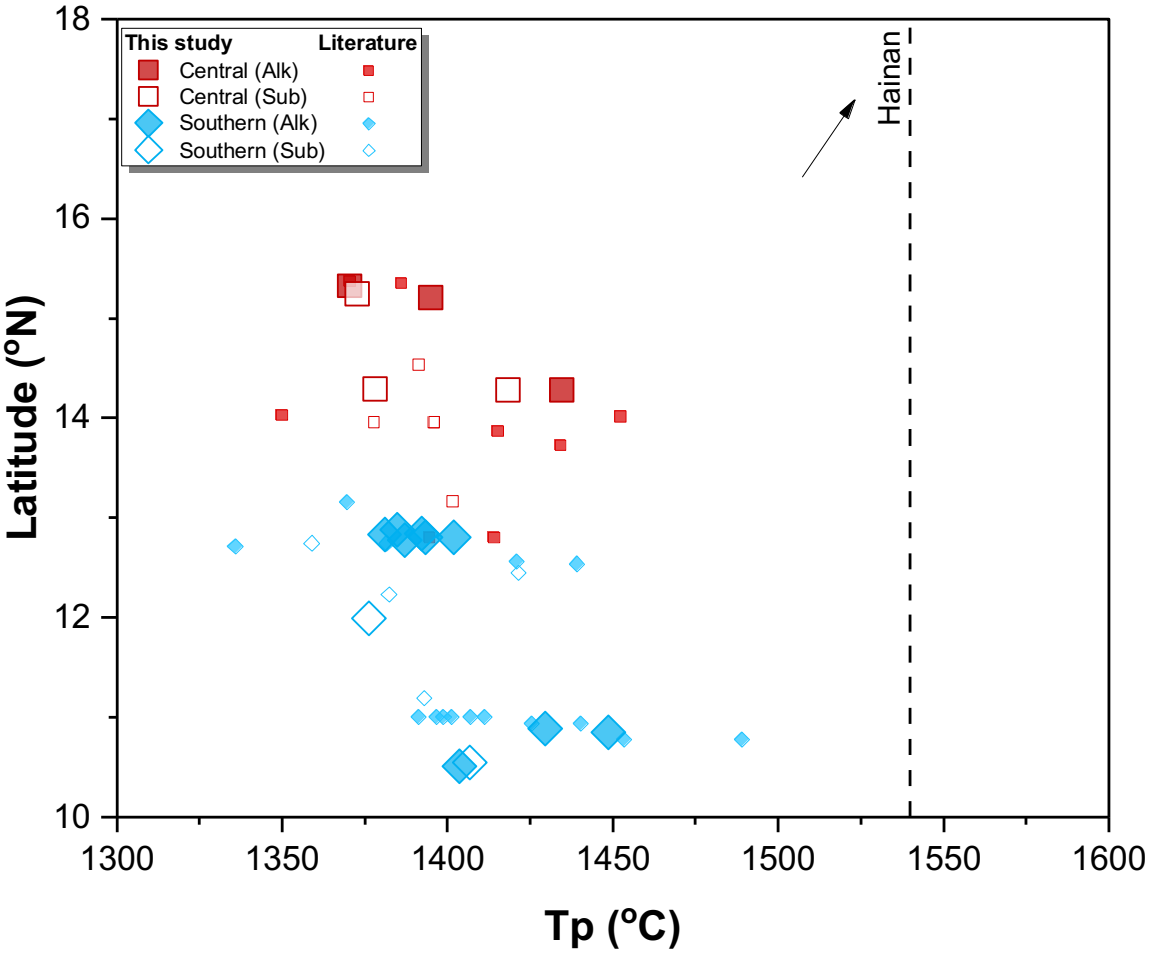

Figure S12: Latitudinal variations in mantle potential temperature (T_p) in the production of parental magmas of Vietnamese basalts. The T_p shown are calculated from melting P and T (P_3 and T_3) in Figure S11 by the algorithm of Plank & Forsyth (2016) and adiabatic gradient of Katz et al. (2003). The average T_p = 1540°C of Hainan basalts is from Wang et al. (2012). Literature data used for calculation are the same as in Figure S9.

Captions for Table S1 to S9 (files uploaded separately)

Table S1. Locality, major- and trace-element concentrations, and Sr-Nd-Pb isotopic compositions of Vietnamese volcanic rocks (Con Co, Ly Son-Quang Ngai, Kong Plong, Pleiku, Buon Ma Thuot, Phuoc Long, Xuan Loc and Phu Quy) and seafloor basalts from the EVS/SCS. Results of replicated ICP-MS analysis of the in-house standard rock MYK-1.

Table S2. CIPW normative compositions.

Table S3. Results of K-Ar dating for the volcanic rocks from Vietnam.

Table S4. K-Ar ages obtained for the reference standard materials.

Table S5. *F* test statistics of the Pb isotope regression trends for Vietnamese basalts.

Table S6. Trace element and isotope compositions of proposed end-member components.

Table S7. a) Parental magma (PM, this study) and wallrock (WR, Owada et al., 2007; Shellnutt et al., 2013) compositions, and input parameters for the AFC model using the Magma Chamber Simulator (Borhson et al., 2014, 2020; Heinonen et al., 2020). b) Partition coefficients for trace elements used in AFC modeling (Adam & Green, 2006; Bacon & Druitt, 1988; Bea et al., 1994; Elkins et al., 2008; Klemme et al., 2006; McKenzi & Onion, 1991; Pilet et al., 2011; Ronov & Yaroshevskiy, 1976).

Table S8. Major-element compositions of primary magmas of Vietnamese basalts (equilibrated with Fo_{90}) and estimated melting pressure (*P*) and temperature (*T*) by thermobarometry.

Table S9. Input parameters for REEBOX PRO model (Brown & Lesher, 2016).

References

Adam, J., & Green, T. (2006). Trace element partitioning between mica- and amphibole-bearing garnet lherzolite and hydrous basanitic melt: 1. Experimental results and the investigation of controls on partitioning behaviour. *Contributions to Mineralogy and Petrology*, *152*(1), 1–17. https://doi.org/10.1007/s00410-006-0085-4

An, A.-R., Choi, S. H., Yu, Y., & Lee, D.-C. (2017). Petrogenesis of Late Cenozoic basaltic rocks from southern Vietnam. *Lithos*, *272–273*, 192–204. https://doi.org/10.1016/j.lithos.2016.12.008

Bacon, C. R., & Druitt, T. H. (1988). Compositional evolution of the zoned calcalkaline magma chamber of Mount Mazama, Crater Lake, Oregon. *Contributions to Mineralogy and Petrology*, *98*(2), 224–256. https://doi.org/10.1007/BF00402114

Barr, S. M., & Macdonald, A. S. (1981). Geochemistry and geochronology of late Cenozoic basalts of Southeast Asia. *Geological Society of America Bulletin*, *92(8_Part_II)*, 1069-1142. https://doi.org/10.1130/GSAB-P2-92-1069

Barr, S. M., & Cooper, M. A. (2013). Late Cenozoic basalt and gabbro in the subsurface in the Phetchabun Basin, Thailand: Implications for the Southeast Asian Volcanic Province. *Journal of Asian Earth Sciences*, *76,* 169-184. https://doi.org/10.1016/j.jseaes.2013.01.013

Beattie, P. (1994). Systematics and energetics of trace-element partitioning between olivine and silicate melts: Implications for the nature of mineral/melt partitioning. *Chemical Geology*, *117(1-4)*, 57–71. https://doi.org/10.1016/0009-2541(94)90121-X

Ben Othman, D., White, W. M., & Patchett, J. (1989). The geochemistry of marine sediments, island arc magma genesis, and crust-mantle recycling. *Earth and Planetary Science Letters*, *94(1–2)*, 1–21. https://doi.org/10.1016/0012-821X(89)90079-4

Blundy, J., Melekhova, E., Ziberna, L., Humphreys, M., Cerantola, V., Brooker, R. A., McCammon, C. A., Pichavant, M. & Ulmer, P. (2020). Effect of redox on Fe–Mg–Mn exchange between olivine and melt and an oxybarometer for basalts. *Contributions to Mineralogy and Petrology*, 175(11), 1–32. https://doi.org/10.1007/s00410-020-01736-7

Bohrson, W. A., Spera, F. J., Ghiorso, M. S., Brown, G. A., Creamer, J. B. & Mayfield, A. (2014). Thermodynamic model for energy-constrained open-system evolution of crustal magma bodies undergoing simultaneous recharge, assimilation and crystallization: the Magma Chamber Simulator. *Journal of Petrology*, 55(9), 1685–1717. https://doi.org/10.1093/petrology/egu036

Bohrson, W. A., Spera, F. J., Heinonen, J. S., Brown, G. A., Scruggs, M. A., Adams, J. V., Takach, M. K., Zeff, G. & Suikkanen, E. (2020). Diagnosing open-system magmatic processes using the Magma Chamber Simulator (MCS): part I—major elements and

phase equilibria. *Contributions to Mineralogy and Petrology*, 175(11), 1–29. https://doi.org/10.1007/s00410-020-01722-z

Brown, E. L., & Lesher, C. E. (2016). REEBOX PRO: A forward model simulating melting of thermally and lithologically variable upwelling mantle. *Geochemistry, Geophysics, Geosystems*, *17*(10), 3929–3968. https://doi.org/10.1002/2016GC006579

Cabral, R. A., Jackson, M. G., Koga, K. T., Rose-Koga, E. F., Hauri, E. H., Whitehouse, M. J., Price, A. A., Day, J. M., Shimizu, N. & Kelley, K. A. (2014). Volatile cycling of H_2O, CO_2, F, and Cl in the HIMU mantle: A new window provided by melt inclusions from oceanic hot spot lavas at Mangaia, Cook I slands. *Geochemistry, Geophysics, Geosystems*, 15(11), 4445–4467. https://doi.org/10.1002/2014GC005473

Condamine, P., Médard, E., & Devidal, J.-L. (2016). Experimental melting of phlogopite-peridotite in the garnet stability field. *Contributions to Mineralogy and Petrology*, *171*(11), 95. https://doi.org/10.1007/s00410-016-1306-0

Danyushevsky, L. V., Eggins, S. M., Falloon, T. J., & Christie, D. M. (2000). H_2O Abundance in Depleted to Moderately Enriched Mid-ocean Ridge Magmas; Part I: Incompatible Behaviour, Implications for Mantle Storage, and Origin of Regional Variations. *Journal of Petrology*, *41*(8), 1329–1364. https://doi.org/10.1093/petrology/41.8.1329

Dasgupta, R., Hirschmann, M. M. & Stalker, K. (2006). Immiscible transition from carbonate-rich to silicate-rich melts in the 3 GPa melting interval of eclogite + CO_2 and genesis of silica-undersaturated ocean island lavas. *Journal of Petrology*, 47(4), 647–671. https://doi.org/10.1093/petrology/egi088

Dasgupta, R., Hirschmann, M. M. & Smith, N.D. (2007). Partial melting experiments of peridotite+ CO_2 at 3 GPa and genesis of alkalic ocean island basalts. *Journal of Petrology*, 48(11), 2093–2124. https://doi.org/10.1093/petrology/egm053

Dasgupta, R., Mallik, A., Tsuno, K., Withers, A. C., Hirth, G., & Hirschmann, M. M. (2013). Carbon-dioxide-rich silicate melt in the Earth's upper mantle. *Nature*, 493(7431), 211–215. https://doi.org/10.1038/nature11731

Davis, F. A., Hirschmann, M. M., & Humayun, M. (2011). The composition of the incipient partial melt of garnet peridotite at 3 GPa and the origin of OIB. *Earth and Planetary Science Letters*, 308(3), 380–390. https://doi.org/10.1016/j.epsl.2011.06.008

Davis, Fred A., & Hirschmann, M. M. (2013). The effects of K_2O on the compositions of near-solidus melts of garnet peridotite at 3 GPa and the origin of basalts from enriched mantle. *Contributions to Mineralogy and Petrology*, 166(4), 1029–1046. https://doi.org/10.1007/s00410-013-0907-0

Dixon, J. E., Leist, L., Langmuir, C., & Schilling, J.-G. (2002). Recycled dehydrated lithosphere observed in plume-influenced mid-ocean-ridge basalt. *Nature*, 420(6914), 385–389. https://doi.org/10.1038/nature01215

Elkins, L. J., Gaetani, G. A., & Sims, K. W. W. (2008). Partitioning of U and Th during garnet pyroxenite partial melting: Constraints on the source of alkaline ocean island basalts. *Earth and Planetary Science Letters*, *265*(1), 270–286. https://doi.org/10.1016/j.epsl.2007.10.034

Falloon, T. J., & Danyushevsky, L. V. (2000). Melting of Refractory Mantle at 1.5, 2 and 2.5 GPa under Anhydrous and H_2O-undersaturated Conditions: Implications for the Petrogenesis of High-Ca Boninites and the Influence of Subduction Components on Mantle Melting. *Journal of Petrology*, *41*(2), 257–283. https://doi.org/10.1093/petrology/41.2.257

Foley, S. F., Prelevic, D., Rehfeldt, T. & Jacob, D. E. (2013). Minor and trace elements in olivines as probes into early igneous and mantle melting processes. *Earth and Planetary Science Letters*, 363, 181–191. https://doi.org/10.1016/j.epsl.2012.11.025

Gale, A., Dalton, C. A., Langmuir, C. H., Su, Y., & Schilling, J.-G. (2013). The mean composition of ocean ridge basalts. *Geochemistry, Geophysics, Geosystems*, *14*(3), 489–518. https://doi.org/10.1029/2012GC004334

Gavrilenko, M., Herzberg, C., Vidito, C., Carr, M. J., Tenner, T. & Ozerov, A. (2016). A calcium-in-olivine geohygrometer and its application to subduction zone magmatism. Journal of Petrology, 57(9), 1811–1832. https://doi.org/10.1093/petrology/egw062

Hauff, F., Hoernle, K. & Schmidt, A. (2003). Sr-Nd-Pb composition of Mesozoic Pacific oceanic crust (Site 1149 and 801, ODP Leg 185): Implications for alteration of ocean crust and the input into the Izu-Bonin-Mariana subduction system. *Geochemistry, Geophysics, Geosystems,* 4(8), 8913. https://doi.org/10.1029/2002GC000421

Heinonen, J. S., Bohrson, W. A., Spera, F. J., Brown, G. A., Scruggs, M. A. & Adams, J. V. (2020). Diagnosing open-system magmatic processes using the Magma Chamber Simulator (MCS): part II—trace elements and isotopes. Contributions to Mineralogy and Petrology, 175(11), 1–21. https://doi.org/10.1007/s00410-020-01718-9

Herzberg, C., & Asimow, P. D. (2015). PRIMELT3 MEGA.XLSM software for primary magma calculation: Peridotite primary magma MgO contents from the liquidus to the solidus. *Geochemistry, Geophysics, Geosystems*, *16*(2), 563–578. https://doi.org/10.1002/2014GC005631

Hirose, K., & Kawamura, K. (1994). A new experimental approach for incremental batch melting of peridotite at 1.5 GPa. *Geophysical Research Letters*, *21*(19), 2139–2142. https://doi.org/10.1029/94GL01792

Hirose, K., & Kushiro, I. (1993). Partial melting of dry peridotites at high pressures: Determination of compositions of melts segregated from peridotite using aggregates of diamond. *Earth and Planetary Science Letters*, *114*(4), 477–489. https://doi.org/10.1016/0012-821X(93)90077-M

Hirose, K. (1997). Partial melt compositions of carbonated peridotite at 3 GPa and role of CO_2 in alkali-basalt magma generation. *Geophysical Research Letters*, *24*(22), 2837–2840. https://doi.org/10.1029/97GL02956

Hirose, K., & Kushiro, I. (1998). The effect of melt segregation on polybaric mantle melting: Estimation from the incremental melting experiments. *Physics of the Earth and Planetary Interiors*, *107*(1), 111–118. https://doi.org/10.1016/S0031-9201(97)00129-5

Hirschmann, M. M., Kogiso, T., Baker, M. B., & Stolper, E. M. (2003). Alkalic magmas generated by partial melting of garnet pyroxenite. *Geology*, *31*(6), 481–484. https://doi.org/10.1130/0091-7613(2003)031<0481:AMGBPM>2.0.CO;2

Hirschmann, M. M. (2018). Comparative deep Earth volatile cycles: The case for C recycling from exosphere/mantle fractionation of major (H_2O, C, N) volatiles and from H_2O/Ce, CO_2/Ba, and CO_2/Nb exosphere ratios. *Earth and Planetary Science Letters*, *502*, 262–273. https://doi.org/10.1016/j.epsl.2018.08.023

Ho, K. S., Chen, J. C., & Juang, W. S. (2000). Geochronology and geochemistry of late Cenozoic basalts from the Leiqiong area, southern China. *Journal of Asian Earth Sciences*, 18(3), 307–324. https://doi.org/10.1016/S1367-9120(99)00059-0

Hoang, N., & Flower, M. (1998). Petrogenesis of Cenozoic basalts from Vietnam: implication for origins of a 'diffuse igneous province.' *Journal of Petrology*, *39*(3), 369–395.

Hoang, N., Flower, M. F. J., & Carlson, R. W. (1996). Major, trace element, and isotopic compositions of Vietnamese basalts: Interaction of hydrous EM1-rich asthenosphere with thinned Eurasian lithosphere. *Geochimica et Cosmochimica Acta*, *60*(22), 4329–4351. https://doi.org/10.1016/S0016-7037(96)00247-5

Hoàng, N., Flower, M. F. J., Chí, C. T., Xuân, P. T., Quý, H. V., & Sơn, T. T. (2013). Collision-induced basalt eruptions at Pleiku and Buôn Mê Thuột, south-central Viet Nam. *Journal of Geodynamics*, *69*, 65–83. https://doi.org/10.1016/j.jog.2012.03.012

Hoang, N., Shinjo, R., Phuc, L. T., Anh, L. D., Huong, T. T., Pécskay, Z., & Bac, D. T. (2019). Pleistocene basaltic volcanism in the Krông Nô area and vicinity, Dac Nong Province (Vietnam). *Journal of Asian Earth Sciences*, *181*, 103903. https://doi.org/10.1016/j.jseaes.2019.103903

Hoang, T. H. A., Choi, S. H., Yu, Y., Pham, T. H., Nguyen, K. H., & Ryu, J.-S. (2018). Geochemical constraints on the spatial distribution of recycled oceanic crust in the mantle source of late Cenozoic basalts, Vietnam. *Lithos*, *296–299*, 382–395. https://doi.org/10.1016/j.lithos.2017.11.020

Hoernle, K., Hauff, F., Werner, R., van den Bogaard, P., Gibbons, A. D., Conrad, S., & Müller, R. D. (2011). Origin of Indian Ocean Seamount Province by shallow recycling of continental lithosphere. *Nature Geoscience*, *4*(12), 883–887. https://doi.org/10.1038/ngeo1331

Jiang, W., Yu, J.H., Wang, X., Griffin, W.L., Pham, T., Nguyen, D. & Wang, F. (2020). Early Paleozoic magmatism in northern Kontum Massif, Central Vietnam: Insights into tectonic evolution of the eastern Indochina Block. Lithos, 376-377, https://doi.org/10.1016/j.lithos.2020.105750.

Katz, R. F., Spiegelman, M., & Langmuir, C. H. (2003). A new parameterization of hydrous mantle melting. *Geochemistry, Geophysics, Geosystems*, *4*(9). https://doi.org/10.1029/2002GC000433

Keshav, S., Gudfinnsson, G. H., Sen, G., & Fei, Y. (2004). High-pressure melting experiments on garnet clinopyroxenite and the alkalic to tholeiitic transition in ocean-island basalts. *Earth and Planetary Science Letters*, *223*(3), 365–379. https://doi.org/10.1016/j.epsl.2004.04.029

Klemme, S., Günther, D., Hametner, K., Prowatke, S., & Zack, T. (2006). The partitioning of trace elements between ilmenite, ulvospinel, armalcolite and silicate melts with implications for the early differentiation of the moon. *Chemical Geology*, *234*(3), 251–263. https://doi.org/10.1016/j.chemgeo.2006.05.005

Kogiso, T., Hirschmann, M. M., & Frost, D. J. (2003). High-pressure partial melting of garnet pyroxenite: possible mafic lithologies in the source of ocean island basalts. *Earth and Planetary Science Letters*, *216*(4), 603–617. https://doi.org/10.1016/S0012-821X(03)00538-7

Koszowska, E., Wolska, A., Zuchiewicz, W., Cuong, N. Q., & Pécskay, Z. (2007). Crustal contamination of Late Neogene basalts in the Dien Bien Phu Basin, NW Vietnam: Some insights from petrological and geochronological studies. *Journal of Asian Earth Sciences*, 29(1), 1–17. https://doi.org/10.1016/j.jseaes.2005.12.003

Krolikowska-Ciaglo, S., Hauff, F. & Hoernle, K. (2005). Sr-Nd isotope systematics in 14–28 Ma low-temperature altered mid-ocean ridge basalt from the Australian Antarctic Discordance, Ocean Drilling Program Leg 187. Geochemistry, Geophysics, Geosystems, 6(1), Q01001, https://doi.org/10.1029/2004GC000802.

Kuritani, T., & Nakamura, E. (2002). Precise isotope analysis of nanogram-level Pb for natural rock samples without use of double spikes. *Chemical Geology*, *186*(1), 31–43. https://doi.org/10.1016/S0009-2541(02)00004-9

Kuritani, T., & Nakamura, E. (2003). Highly precise and accurate isotopic analysis of small amounts of Pb using ^{205}Pb-^{204}Pb and ^{207}Pb-^{204}Pb, two double spikes. *Journal of Analytical Atomic Spectrometry*, *18*(12), 1464–1470. https://doi.org/10.1039/B310294G

Kushiro, I. (1996). Partial melting of fertile mantle peridotite at high pressures: an experimental study using aggregates of diamond. *Geophysical Monograph-American Geophysical Union*, *95*, 109–122.

Lambart, S., Laporte, D., & Schiano, P. (2009a). An experimental study of pyroxenite partial melts at 1 and 1.5 GPa: Implications for the major-element composition of Mid-Ocean Ridge Basalts. *Earth and Planetary Science Letters*, *288*(1), 335–347. https://doi.org/10.1016/j.epsl.2009.09.038

Lambart, S., Laporte, D., & Schiano, P. (2009b). An experimental study of focused magma transport and basalt–peridotite interactions beneath mid-ocean ridges: implications for

930 the generation of primitive MORB compositions. *Contributions to Mineralogy and*
931 *Petrology*, *157*(4), 429–451. https://doi.org/10.1007/s00410-008-0344-7

932 Lambart, S., Laporte, D., Provost, A., & Schiano, P. (2012). Fate of Pyroxenite-derived Melts
933 in the Peridotitic Mantle: Thermodynamic and Experimental Constraints. *Journal of*
934 *Petrology*, *53*(3), 451–476. https://doi.org/10.1093/petrology/egr068

935 Lambart, S., Laporte, D., & Schiano, P. (2013). Markers of the pyroxenite contribution in the
936 major-element compositions of oceanic basalts: Review of the experimental
937 constraints. *Lithos*, *160–161*, 14–36. https://doi.org/10.1016/j.lithos.2012.11.018

938 Lan, C. Y., Chung, S. L., Van Long, T., Lo, C. H., Lee, T. Y., Mertzman, S. A., & Jiun-San
939 Shen, J. (2003). Geochemical and Sr–Nd isotopic constraints from the Kontum
940 massif, central Vietnam on the crustal evolution of the Indochina block. *Precambrian*
941 *Research*, 122(1-4), 7–27. https://doi.org/10.1016/S0301-9268(02)00205-X

942 Le, D. A., Nguyen, H., Phung, V. P., Dinh, Q. S., & Shakirov, R. (2019). Geochemical
943 features of olivines from Northeastern Phu Quy Volcanic Island and their relation to
944 melt variations in the magma source. *Journal of Geology (Geological Survey of*
945 *Vietnam)*, Series B (49–50), 1–18.

946 Lee, C.-T. A., Luffi, P., Plank, T., Dalton, H., & Leeman, W. P. (2009). Constraints on the
947 depths and temperatures of basaltic magma generation on Earth and other terrestrial
948 planets using new thermobarometers for mafic magmas. *Earth and Planetary Science*
949 *Letters*, *279*(1), 20–33. https://doi.org/10.1016/j.epsl.2008.12.020

950 Lee, T., Lo, C.-H., Chung, S.-L., Chen, C.-Y., Wang, P.-L., Lin, W.-P., et al. (1998).
951 $^{40}Ar/^{39}Ar$ Dating Result of Neogene Basalts in Vietnam and its Tectonic Implication.
952 *Mantle Geodynamics and Plate Interactions in East Asia, AGU Monograph*, *27*, 317–
953 330. https://doi.org/10.1029/GD027p0317

954 Lepvrier, C., Maluski, H., Van Tich, V., Leyreloup, A., Thi, P.T. & Van Vuong, N. (2004).
955 The early Triassic Indosinian orogeny in Vietnam (Truong Son Belt and Kontum
956 Massif); implications for the geodynamic evolution of Indochina. Tectonophysics,
957 393(1-4), 87–118. https://doi.org/10.1016/j.tecto.2004.07.030

958 Lu, Y., Makishima, A., & Nakamura, E. (2007). Coprecipitation of Ti, Mo, Sn and Sb with
959 fluorides and application to determination of B, Ti, Zr, Nb, Mo, Sn, Sb, Hf and Ta by
960 ICP-MS. *Chemical Geology*, *236*(1), 13–26.
961 https://doi.org/10.1016/j.chemgeo.2006.08.007

962 Makishima, A., & Nakamura, E. (2006). Determination of Major/ Minor and Trace Elements
963 in Silicate Samples by ICP-QMS and ICP-SFMS Applying Isotope Dilution-Internal
964 Standardisation (ID-IS) and Multi-Stage Internal Standardisation. *Geostandards and*
965 *Geoanalytical Research*, *30*(3), 245–271. https://doi.org/10.1111/j.1751-
966 908X.2006.tb01066.x

967 Makishima, A., Nath, B. N., & Nakamura, E. (2008). New sequential separation procedure
968 for Sr, Nd and Pb isotope ratio measurement in geological material using MC-ICP-

MS and TIMS. *Geochemical Journal*, *42*(3), 237–246. https://doi.org/10.2343/geochemj.42.237

Maluski, H., Lepvrier, C., Leyreloup, A., Van Tich, V. & Thi, P.T. (2005). ^{40}Ar–^{39}Ar geochronology of the charnockites and granulites of the Kan Nack complex, Kon Tum Massif, Vietnam. Journal of Asian Earth Sciences, 25(4), 653–677. https://doi.org/10.1016/j.jseaes.2004.07.004

McDonough, W. F., & Sun, S. -s. (1995). The composition of the Earth. *Chemical Geology*, *120*(3–4), 223–253. https://doi.org/10.1016/0009-2541(94)00140-4

McKenzie, D. & O'Nions, R.K. (1991). Partial melt distributions from inversion of rare earth element concentrations. *Journal of Petrology*, 32(5), 1021–1091. https://doi.org/10.1093/petrology/32.5.1021

Michael, P. (1995). Regionally distinctive sources of depleted MORB: Evidence from trace elements and H_2O. *Earth and Planetary Science Letters*, *131*(3), 301–320. https://doi.org/10.1016/0012-821X(95)00023-6

Nagao, K., Ogata, A., Miura, Y. N., & Yamaguchi, K. (1996). Ar isotope analysis for K-Ar dating using two modified-VG5400 mass spectrometers—I: Isotope dilution method. *Journal of the Mass Spectrometry Society of Japan*, *44*(1), 39–61. https://doi.org/10.5702/massspec.44.39

Nakamura, E., McDougall, I., & Campbell, I. H. (1986). K-Ar ages of basalts from the Higashi-Matsuura district, northwestern Kyushu, Japan and regional geochronology of the Cenozoic alkaline volcanic rocks in eastern Asia. *Geochemical Journal*, *20*(2), 91–99. https://doi.org/10.2343/geochemj.20.91

Nakamura, E., Makishima, A., Moriguti, T., Kobayashi, K., Sakaguchi, C., Yokoyama, T., et al. (2003). Comprehensive geochemical analyses of small amounts (< 100 mg) of extraterrestrial samples for the analytical competition related to the sample return mission MUSES-C. *Inst. Space Astronaut. Sci. Rep. SP.*, *16*, 49–101.

Nguyen, H. H., Pham, N. S., Hoang, V. L., Andrew, C., Bui, V. H., Bui, H. B., Trinh, T. T., & Nguyen, L. A. (2021). Cretaceous Granitic Magmatism in South-Central Vietnam: Constraints from zircon U–Pb geochronology. Inżynieria Mineralna – Journal of the Polish Mineral Engineering Society, 1(2), 7–14. https://doi.org/10.29227/IM-2021-02-01

Nguyen, T. T., Kitagawa, H., Pineda-Velasco, I., & Nakamura, E. (2020). Feedback of Slab Distortion on Volcanic Arc Evolution: Geochemical Perspective From Late Cenozoic Volcanism in SW Japan. *Journal of Geophysical Research: Solid Earth*, *125*(10), e2019JB019143. https://doi.org/10.1029/2019JB019143

Nguyen, T. T. B., Satir, M., Siebel, W., Vennemann, T. & Van Long, T. (2004a). Geochemical and isotopic constraints on the petrogenesis of granitoids from the Dalat zone, southern Vietnam. Journal of Asian Earth Sciences, 23(4), 467–482. https://doi.org/10.1016/j.jseaes.2003.06.001

Nguyen, T. T. B., Satir, M., Siebel, W. & Chen, F. (2004b). Granitoids in the Dalat zone, southern Vietnam: age constraints on magmatism and regional geological implications. International Journal of Earth Sciences, 93(3), 329–340. https://doi.org/10.1007/s00531-004-0387-6

Nier, A. O. (1950). A redetermination of the relative abundances of the isotopes of carbon, nitrogen, oxygen, argon, and potassium. Physical Review, 77(6), 789–793. https://doi.org/10.1103/PhysRev.77.789

Owada, M., Osanai, Y., Nakano, N., Matsushita, T., Nam, T. N., Tsunogae, T., Toyoshima, T., Binh, P. & Kagami, H. (2007). Crustal anatexis and formation of two types of granitic magmas in the Kontum massif, central Vietnam: Implications for magma processes in collision zones. Gondwana Research, 12(4), 428–437. https://doi.org/10.1016/j.gr.2006.11.001

Patte, É. (1925). Étude de l'île des Cendres, volcan apparu au large de la côte d'Annam, par Étienne Patte. Impr. d'Extrême-Orient. Bulletin du Service G´eologique de l'Indochine 13, 1–19.

Pickering-Witter, J., & Johnston, A. D. (2000). The effects of variable bulk composition on the melting systematics of fertile peridotitic assemblages. *Contributions to Mineralogy and Petrology*, *140*(2), 190–211. https://doi.org/10.1007/s004100000183

Pilet, S., Baker, M. B., Müntener, O., & Stolper, E. M. (2011). Monte Carlo Simulations of Metasomatic Enrichment in the Lithosphere and Implications for the Source of Alkaline Basalts. *Journal of Petrology*, *52*(7–8), 1415–1442. https://doi.org/10.1093/petrology/egr007

Plank, T., & Forsyth, D. W. (2016). Thermal structure and melting conditions in the mantle beneath the Basin and Range province from seismology and petrology. *Geochemistry, Geophysics, Geosystems*, *17*(4), 1312–1338. https://doi.org/10.1002/2015GC006205

Plank, T., & Langmuir, C. H. (1998). The chemical composition of subducting sediment and its consequences for the crust and mantle. *Chemical Geology*, *145*(3–4), 325–394. https://doi.org/10.1016/S0009-2541(97)00150-2

Putirka, K. D. (2008). Thermometers and Barometers for Volcanic Systems. *Reviews in Mineralogy and Geochemistry*, *69*(1), 61–120. https://doi.org/10.2138/rmg.2008.69.3

Rangin, C., Huchon, P., Le Pichon, X., Bellon, H., Lepvrier, C., Roques, D., Hoe, N.D. & Van Quynh, P. (1995). Cenozoic deformation of central and south Vietnam. *Tectonophysics*, 251(1-4), 179–196. https://doi.org/10.1016/0040-1951(95)00006-2

Roeder, P. L., & Emslie, R. F. (1970). Olivine-liquid equilibrium. Contributions to Mineralogy and Petrology, 29(4), 275–289. https://doi.org/10.1007/BF00371276

Ronov, A. B., & Yaroshevskiy, A. A. (1976). A new model for the chemical structure of the Earth's crust. *Geochemistry International*, *13*(6), 89–121.

Salters, V. J. M., & Stracke, A. (2004). Composition of the depleted mantle. *Geochemistry, Geophysics, Geosystems*, *5*(5). https://doi.org/10.1029/2003GC000597

Sieh, K., Herrin, J., Jicha, B., Angel, D.S., Moore, J.D., Banerjee, P., Wiwegwin, W., Sihavong, V., Singer, B., Chualaowanich, T., & Charusiri, P. (2020). Australasian impact crater buried under the Bolaven volcanic field, Southern Laos. Proceedings of the National Academy of Sciences, 117(3), 1346–1353. https://doi.org/10.1073/pnas.1904368116

Shellnutt, J. G., Lan, C. Y., Van Long, T., Usuki, T., Yang, H. J., Mertzman, S. A., Iizuka, Y., Chung, S. L., Wang, K. L., & Hsu, W. Y. (2013). Formation of Cretaceous Cordilleran and post-orogenic granites and their microgranular enclaves from the Dalat zone, southern Vietnam: Tectonic implications for the evolution of Southeast Asia. *Lithos*, 182-183, 229–241. https://doi.org/10.1016/j.lithos.2013.09.016

Sobolev, A. V., Hofmann, A. W., Sobolev, S. V., & Nikogosian, I. K. (2005). An olivine-free mantle source of Hawaiian shield basalts. Nature, 434(7033), 590–597. https://doi.org/10.1038/nature03411

Sobolev, A. V., Hofmann, A. W., Kuzmin, D. V., Yaxley, G. M., Arndt, N. T., Chung, S.-L., et al. (2007). The Amount of Recycled Crust in Sources of Mantle-Derived Melts. Science, 316(5823), 412–417. https://doi.org/10.1126/science.1138113

Steiger, R. H., & Jäger, E. (1977). Subcommission on geochronology: Convention on the use of decay constants in geo- and cosmochronology. *Earth and Planetary Science Letters*, *36*(3), 359–362. https://doi.org/10.1016/0012-821X(77)90060-7

Stracke, A., Hofmann, A. W., & Hart, S. R. (2005). FOZO, HIMU, and the rest of the mantle zoo. *Geochemistry, Geophysics, Geosystems*, *6*(5). https://doi.org/10.1029/2004GC000824

Takei, H. (2002). Development of precise analytical techniques for major and trace element concentrations in rock samples and their applications to the Hishikari Gold Mine, southern Kyushu, Japan. *Ph. D Thesis, Okayama University*.

Tanaka, R., Makishima, A., Kitagawa, H., & Nakamura, E. (2003). Suppression of Zr, Nb, Hf and Ta coprecipitation in fluoride compounds for determination in Ca-rich materials. *Journal of Analytical Atomic Spectrometry*, *18*(12), 1458–1463. https://doi.org/10.1039/B309948B

Tran, T. H., Lan, C. Y., Usuki, T., Shellnutt, J. G., Pham, T. D., Tran, T. A., Pham, N. C., Ngo, T. P., Izokh, A. E. & Borisenko, A. S. (2015). Petrogenesis of Late Permian silicic rocks of Tu Le basin and Phan Si Pan uplift (NW Vietnam) and their association with the Emeishan large igneous province. *Journal of Asian Earth Sciences*, 109, 1–19. https://doi.org/10.1016/j.jseaes.2015.05.009

Walter, M. J. (1998). Melting of Garnet Peridotite and the Origin of Komatiite and Depleted Lithosphere. *Journal of Petrology*, *39*(1), 29–60. https://doi.org/10.1093/petroj/39.1.29

Wang, X.-C., Li, Z.-X., Li, X.-H., Li, J., Liu, Y., Long, W.-G., Zhou, J.-B. & Wang, F. (2012). Temperature, pressure, and composition of the mantle source region of Late Cenozoic basalts in Hainan Island, SE Asia: a consequence of a young thermal mantle

plume close to subduction zones? *Journal of Petrology*, 53(1), 177–233. https://doi.org/10.1093/petrology/egr061

Workman, R. K., & Hart, S. R. (2005). Major and trace element composition of the depleted MORB mantle (DMM). *Earth and Planetary Science Letters*, *231*(1), 53–72. https://doi.org/10.1016/j.epsl.2004.12.005

Yang, Z.-F., Li, J., Jiang, Q.-B., Xu, F., Guo, S.-Y., Li, Y., & Zhang, J. (2019). Using Major Element Logratios to Recognize Compositional Patterns of Basalt: Implications for Source Lithological and Compositional Heterogeneities. *Journal of Geophysical Research: Solid Earth*, *124*(4), 3458–3490. https://doi.org/10.1029/2018JB016145

Yaxley, G. M. & Green, D. H. (1998). Reactions between eclogite and peridotite: mantle refertilisation by subduction of oceanic crust. Schweizerische Mineralogische und Petrographische Mitteilungen, 78(2), 243–255.

Yokoyama, T., Makishima, A., & Nakamura, E. (1999). Evaluation of the coprecipitation of incompatible trace elements with fluoride during silicate rock dissolution by acid digestion. *Chemical Geology*, *157*(3), 175–187. https://doi.org/10.1016/S0009-2541(98)00206-X

Yoshikawa, M., & Nakamura, E. (1993). Precise isotope determination of trace amounts of Sr in Magnesium-rich samples. *Journal of Mineralogy, Petrology and Economic Geology*, *88*(12), 548–561. https://doi.org/10.2465/ganko.88.548

Zhang, G.-L., Luo, Q., Zhao, J., Jackson, M. G., Guo, L.-S., & Zhong, L.-F. (2018a). Geochemical nature of sub-ridge mantle and opening dynamics of the South China Sea. *Earth and Planetary Science Letters*, *489*, 145–155. https://doi.org/10.1016/j.epsl.2018.02.040

Zhang, G.-L., Sun, W.-D., & Seward, G. (2018b). Mantle Source and Magmatic Evolution of the Dying Spreading Ridge in the South China Sea. *Geochemistry, Geophysics, Geosystems*, *19*(11), 4385–4399. https://doi.org/10.1029/2018GC007570

Zindler, A., & Hart, S. (1986). Chemical Geodynamics. *Annual Review of Earth and Planetary Sciences*, *14*(1), 493–571. https://doi.org/10.1146/annurev.ea.14.050186.002425